LBL-11234
Preprint

Lawrence Berkeley Laboratory
UNIVERSITY OF CALIFORNIA

Materials & Molecular Research Division

Submitted to the Journal of Chemical Physics

ULTRAVIOLET ABSORPTION SPECTRUM OF NITROUS OXIDE AS FUNCTION OF TEMPERATURE AND ISOTOPIC SUBSTITUTION

Gary S. Selwyn and Harold S. Johnston

July 1980

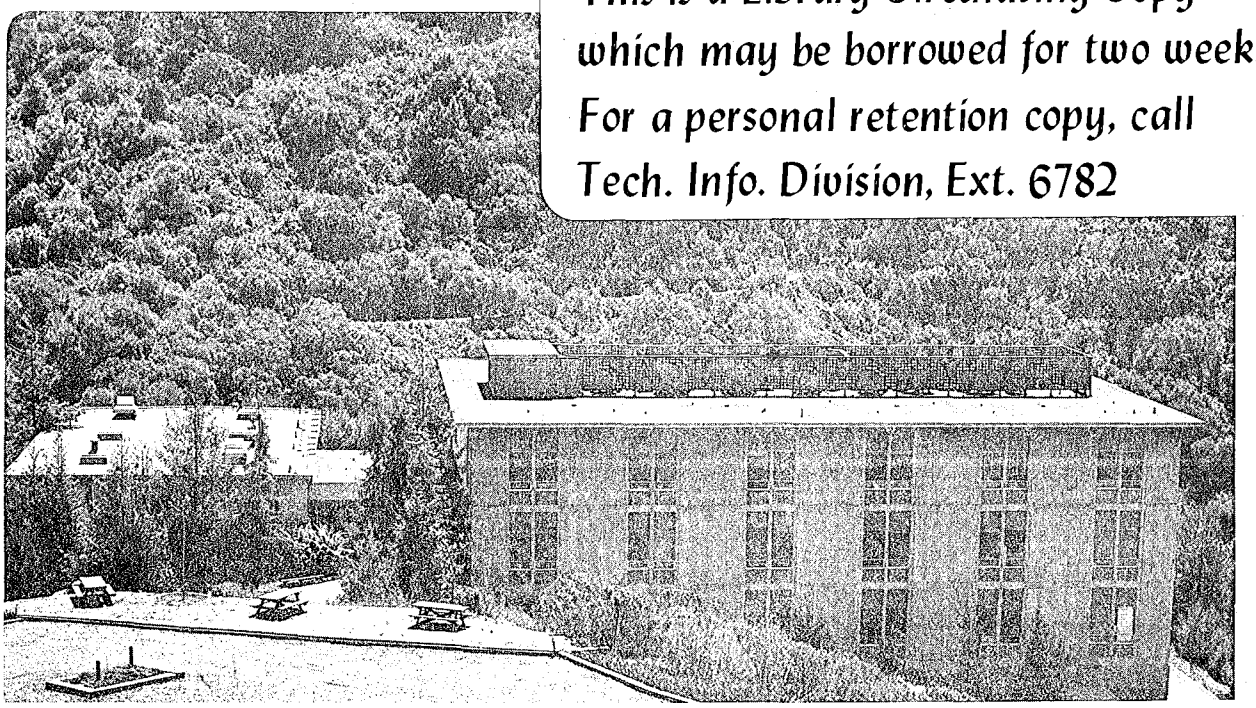

Prepared for the U.S. Department of Energy under Contract W-7405-ENG-48

Ultraviolet Absorption Spectrum of Nitrous Oxide as Function of Temperature and Isotopic Substitution

By

Gary S. Selwyn[†] and Harold S. Johnston

Department of Chemistry, University of California and Materials and Molecular Research Division, Lawrence Berkeley Laboratory, Berkeley, California 94720

Abstract: The ultraviolet absorption spectra of nitrous oxide and its ^{15}N isotopes over the wavelength range 197 to 172 nm and between 150 and 500 K show a weak continuous absorption and a pattern of diffuse banding that become pronounced at higher temperatures. The temperature dependence of the absorption spectrum results from the activation of the ν_2'' bending mode. Deconvolution of the data shows that absorption by molecules in the (010) vibrational mode results in a spectrum of vibrational bands superimposed on a continuum. A weaker and nearly continuous spectrum results from the ultraviolet absorption by molecules in the (000) vibrational mode. Analysis of the structuring indicates $\nu_2' = (490 \pm 10)$ cm^{-1}. No rotational structure can be observed. Measurement of the ν_2' isotope shift is used to identify the quantum number of the upper state vibrational levels. Normal coordinate analysis of the excited state is used to determine a self-consistent set of molecular parameters: bond angle (115°), the values of ν_1' and ν_3' (1372 and 1761 cm^{-1}) and the force constants of the upper state. It is suggested that the transitions observed are $^1\Sigma^-(^1A'') \leftarrow \tilde{X}^1\Sigma^+$ and $^1\Delta \leftarrow \tilde{X}^1\Sigma^+$.

[†]Present address: Division of Chemistry, Code 6110, Naval Research Laboratory, Washington, D.C. 20375

Introduction

The first ultraviolet absorption spectrum of nitrous oxide was reported[1] in 1926. There have been other studies of its near UV spectrum,[2-6] its vacuum UV absorption spectrum,[7-11] and its photodissociation.[12-20] For the region 160 to 240 nm, the concensus of investigators was that there was a continuous absorption centered at about 185 nm with some uncertainty as to the origin on the long wavelength side. Some studies[3,21] indicated a weak absorption at wavelengths longer than 260 nm, but it has been shown that the apparent absorption approaches the Rayleigh scattering limit at these wavelengths.[22] A study in 1940 indicated that the intensity of the 170 to 200 nm absorption spectrum decreased as the temperature was lowered from 298 to 183 K,[5] and a later study showed that the spectrum above 200 nm was increased in intensity and red-shifted as the temperature was increased above room temperature.[4] Weak, diffuse bands superimposed on the continuous absorption centered at 180 nm have been detected,[9,11] but these features were so weak that they could not be accurately measured nor interpreted. The non-optical method of high-resolution electron-energy loss spectra[23,33] has also been used to detect these diffuse bands in N_2O around 6.8 eV, although the bands were too weak and diffuse for analysis by this method.

In a previous publication from this laboratory,[24] the absorption spectrum of nitrous oxide at moderately high resolution was shown to have a banded structure superimposed on a continuous absorption between 174 and 190 nm. The present investigation studies this spectrum as a function of temperature, 150-500 K; and as a function of nitrogen isotopic substitution, $^{14}N^{14}N^{16}O$, $^{14}N^{15}N^{16}O$, $^{15}N^{14}N^{16}O$, and $^{15}N^{15}N^{16}O$.

Experimental

Equipment. A Cary 118C spectrophotometer was modified to accept a bulky cell and to allow efficient nitrogen purging so it could be used down to 170 nm. The deuterium lamp source was also sealed and purged by nitrogen. The spectrophotometer was kept in a purged, oxygen-free condition for the duration of the data collection. Efficiency of the purging was verified by the absence of oxygen bands in the evacuated cell. Rapidly decreasing output of the lamp, optics and detector below 175 nm made data collection at shorter wavelengths increasingly difficult. The analog output of the spectrometer was stored by a Fabritek 1074 data collector with a 12 bit A/D converter and 4000 words of storage space. Data could be arithmetically manipulated by the Fabritek and displayed on an oscilloscope. The Fabritek was interfaced to a PDP 8L minicomputer, where further data reduction was carried out. Data from the minicomputer were stored and transferred to a CDC 7600 computer for further analysis and graphic presentation.

All spectra were obtained in double-beam mode, one beam through the thermostated gas cell and the other through nitrogen in the cell compartment. Alternate spectra were obtained through the evacuated cell and through the cell containing nitrous oxide, in each case to give optical density relative to the reference beam through nitrogen. Wavelength calibration was carried out by addition of O_2 to the cell and observing the rotational structure of the Schumann-Runge oxygen bands.[25] The data collected on a time basis by the Fabritek corresponded to a linear wavelength scale on the Cary 118C and were converted to a vacuum wavenumber basis, $\nu = 10^7(\eta\lambda)^{-1}$ where η is the index of refraction of nitrogen and λ is the wavelength in nanometers.[26] The intensities of the data

presented here are estimated to be accurate to about four percent in absolute cross sections.

A triaxial silica cell, Figure 1, was used. The innermost cell with suprasil windows contained the nitrous oxide being studied. The central jacket was used for temperature control. The outermost compartment, also with suprasil windows, was evacuated and provided thermal insulation. For temperatures below 200 K a stream of cold nitrogen gas boiled off from liquid nitrogen was used to cool the cell. For temperatures between 200 and 373 K a thermostated fluid was circulated through the control jacket. At higher temperatures, the central compartment was filled with silicone oil and heated by passing a controlled current through the platinum wires. This platinum-wire heater was also used to bake out the cell when it was evacuated. Temperature was measured by thermocouples in contact with the inner cell. The nitrous oxide was between 5 and 45 torr, and its pressure was measured with a capacitance manometer (MKS Baratron). As a check on temperature and pressure measurements, the equilibrium vapor pressure of N_2O at temperatures below 183 K was recorded.

First data set. The first set of studies used isotopically normal nitrous oxide, and the primary purpose was to study the effect of temperature on the absorption spectrum. Data were taken at eleven temperatures: 151, 182, 196, 223, 243, 268, 301, 333, 372, 423, and 485 K. The wavelength range was 190 to 172 nm, scan speed was 0.01 nm s^{-1}, slit widths were 0.06 nm to give an average spectral band width of 0.05 nm, and data points were recorded every 0.02 nm with a 5 second time constant. At each temperature four scans of sample and background were repeated and separately stored in the Fabritek 1074. If the scans were

found to be free of drift or other error, the four scans for the sample were averaged and the four scans for the background were averaged. These data were stored for subsequent calculations and interpretations.

Second data set. A second set of studies concerned the effect of isotopic substitution on the ultraviolet absorption spectrum of nitrous oxide. Side-by-side comparisons were made for four isotopic species: $^{14}N^{14}N^{16}O$, $^{15}N^{14}N^{16}O$, $^{14}N^{15}N^{16}O$, and $^{15}N^{15}N^{16}O$. Data were taken at six temperatures: 148, 213, 301, 372, 442, and 503 K. The wavelength range was 197 to 173 nm, the average spectral band width was 0.07 nm, two scans were averaged for each condition, and otherwise experimental conditions were as in the first data set. The three N-15 isotopes were obtained from Prochem, British Oxygen Co., and the stated isotopic purity was 99.% or better. Gas purity and isotopic purity were checked by measuring the infrared spectrum with a Nicolet 7199 fourier transform spectrometer and comparing the results with literature values.[27]

Three meter vacuum spectrograph. One experiment was carried out at reduced pressure and high resolution. The main chamber of a 3 m McPherson 241 spectrograph was evacuated and filled at room temperature with 50 to 250 millitorr of nitrous oxide. Exposures were taken at high resolution, (first order — dispersion 2.79 Å/mm, slit width 10 μm, to give effective band width of $\sim$ 0.003 nm), using Kodak SWR plates and an air cooled deuterium lamp. Wavelength calibration was accomplished by the presence of the sharp rotational line spectra of O_2. Densitometer tracings were made of the plates.

Results

The absorption cross section ($\sigma = C^{-1}L^{-1}$ ln I_o/I, 10^{-19} cm^2) of nitrous oxide is shown in Figure 2 for eleven temperatures between 151 and 485 K. The intensity of the absorption spectrum increases with increasing temperature, by about a factor of 2 at 53000 cm^{-1} and by about a factor of 1.3 at 58000 cm^{-1}. The increase in absorption intensity with increasing temperature has been noted before at longer wavelengths.[4] There appears to be a continuous background spectrum and a weak superimposed banded spectrum. The banded spectrum is fairly well defined at high temperature, but it is indistinct at low temperature. This figure is the point-by-point print-out of the observed data, and the computer-plotting method fails to resolve the different curves when they become of comparable value at high energies.

The spectrum obtained at high resolution (low pressure, room temperature, 3 m grating spectrograph) also demonstrates a continuous background and a weak superimposed banded system. The high resolution spectrograph did not resolve rotational features in the spectrum. The full width at half intensity between peaks and troughs as obtained by the 3 m spectrograph was essentially the same as the corresponding quantity found by the Cary 118C. However, the heights of the peaks relative to the adjacent valleys are two to four times greater at high resolution than at the resolution of the Cary 118C at room temperature.

The absorption cross sections for the four isotopic species (14, 14, 16), (14, 15, 16), (15, 14, 16), and (15, 15, 16) at six temperatures are presented as Figures 3-6. These four figures show the same

qualitative features as Figure 2 but cover a wider wavelength range. The additional range covered at relatively low energies shows some evidence of shoulders, which appear to be a continuation of the banded structure.

A listing of the absorption cross sections at all temperatures is available from the authors or from Reference 45.

Interpretation of Data

Contribution of cold and hot bands of ground electronic state of nitrous oxide. Using the fundamental vibrational frequencies[28] of N_2O (1284, 589, 2223 cm^{-1}), it is possible to calculate the fractional population of vibrational modes in the ground electronic state ($\tilde{X}^1\Sigma^+$) for any given temperature.[29] At the lowest temperature studied, 151 K, 99.3% of the molecules are in the (000) vibrational mode and thus this spectrum provides a good approximation to the ultraviolet spectrum of the "pure" (000) vibrational mode spectrum. Weighting this spectrum by the fractional (000) population for each of the five highest temperatures studied and subtracting the resultant spectral contribution of the (000) molecules from each of these five highest temperature spectra, the difference spectra obtained represent the spectral contributions of the vibrationally "hot" molecules at these temperatures.

It is possible to identify the active vibrational mode which is responsible for these difference spectra by dividing the difference spectra by the fractional equilibrium populations of the exicited vibrational modes of N_2O. Only for the first excited bending mode, (010), with an energy of 589 cm^{-1} are the normalized "hot" spectra consistent and in agreement for all five spectra. Applying the same procedure, but using the energy of $2\nu_2$ or ν_1 yields widely varying normalized results for each of these five highest temperatures,

indicating these modes are not primarily responsible for the observed temperature effect.

An iterative procedure was used to approximate the individual vibrational mode spectra:

$$B(\lambda) = \frac{Y(\lambda,T) - a(T)A(\lambda)}{b(T)} \qquad (1)$$

where $A(\lambda)$ and $B(\lambda)$ are the spectra of the (000) and (010) vibrational modes respectively for 100% occupancy, $Y(\lambda,T)$ is the observed spectrum at temperature T, and $a(T)$ and $b(T)$ are the fractional equilibrium populations of (000) and (010) respectively. Solution of (1) simultaneously to give the (000) and (010) vibrational mode spectra is accomplished through an iterative procedure using each data point of the 151 and 333 K absorption spectra. In the first stage of solution, an approximation to the (010) mode spectrum is derived by the substitution of the 151 K spectrum for the (000) mode spectrum, $A(\lambda)$. With this result, the 151 K spectrum is then corrected for the contribution of the 0.7% of molecules in the (010) vibrational mode at that temperature. The (000) and (010) vibrational mode spectra are then derived through the repeated application of (1). Convergence occurs quickly with the final result shown in Figure 7. The large effect of the bending vibration upon the resultant absorption spectrum of nitrous oxide is apparent in Figure 7. Most of the structuring is seen to result from the excitation of the bending vibration although a small amount of structuring is seen in the (000) spectrum. Comparison of the peak-to-trough intensities of the two spectra shows the intensity of the structuring in the (000) spectrum is $\sim$ 4% of the intensity of structuring from the (010) mode. The

underlying continuum of the (010) spectrum is also enhanced and is red-shifted from the maximum of the (000) spectrum. The presence of a vibrational progression is pronounced in the (010) spectrum.

The reverse process of weighting each state spectrum by the fractional population of (000) and (010) for a given temperature and adding allows a comparison of this composite spectrum and the observed spectrum over a wide temperature range. This procedure is illustrated for temperatures 151, 196, 243, 301, 372, and 485 in Figure 8. The 151 and 333 K spectra were used to derive the two vibrational mode spectra and therefore are not independent comparisons by this method. Figure 8 shows good agreement at some temperatures and fair agreement at other temperatures. This method tends to underestimate the absorption at the highest temperatures because at these temperatures the method ignores the increasingly substantial population and spectral contribution of higher vibrational modes. Similarly, in the derivation of the (010) state spectrum, this method unavoidably includes the interfering contribution of the equilibrium population of (020) at 333 K (about 1%), and so at lower temperatures where there is less (020) population this convolution tends to slightly overestimate the absorption.

Upper state vibrational progression. The absorption spectra in Figure 2 appear to show a fairly well-defined vibrational progression, especially at high temperatures. Even the low-temperature spectra show some reproducible structure. Figure 9 shows the observed spectrum at 151 K, the (000) spectrum as discussed in the previous section, and an empirical energy-weighted Gaussian function, a function appropriate for a continuous absorption[30]

$$I(\lambda) = N \nu \exp[- D(\nu - \nu_o)^2] \qquad (2)$$

where D, N, and ν_o are fitted constants. The energy-weighted Gaussian was adjusted to fall just below the observed valleys between the spectral features. Two such functions were obtained, one for the (000) spectrum and one for the (010) spectrum. At each temperature a curve was obtained as the weighted average of the (000) and (010) Gaussian, and this curve was subtracted from the observed curve to obtain a difference curve that consisted only of peaks and valleys. Examples of these difference curves are given by Figures 10, 11, and 12 at temperatures 151, 333, and 485, respectively. There are well-defined peaks at high temperatures and some reproducible structure at low temperatures. Some of this structure may be vibrational features; some may be unresolved rotational bands; and some is experimental error. A computer program was developed to select the major peaks using the same objective criteria for all temperatures, and it was designed to overlook small features. The peak-selecting program used criteria of peak height, peak width, and inflections in the first-derivative of the plot. Unavoidably, the program would occasionally identify nearby peaks on a feature with a slight double maximum which a more subjective observer would regard as one peak, and occasionally it missed a very sharp peak or a shoulder on an intense peak. The features that the program identified as peaks are indicated by solid vertical lines in Figures 10-12.

One might ask why not apply a peak-selecting program directly to the experimental data, Figure 1. The reason not to proceed this way is indicated by Figure 9. There is a wavelength dependent change in what

the experiment sees as an underlying continuum. Data from the 3 m high-resolution spectrograph show that some of this "underlying continuum" is lack of resolution in the Cary 118C. Even so, it was much easier to develop a uniform, objective peak-selecting program for the difference spectra, Figures 10-12, than for the direct data, Figure 2.

At each of the eleven temperatures, peaks were selected, as illustrated by Figures 10-12. At each temperature the permutations of all energy separations between the selected peaks were measured and counted in bins of 20 cm^{-1}. The summation of this energy-separation count for all eleven temperatures is shown in Figure 13 as a histogram of frequency of occurrence in energy separation between peaks as a function of the relative separation in cm^{-1}. The half-peak above zero wavenumbers corresponds to double counting inside single peaks. Aside from this feature, the histogram appears to show a well-defined vibrational progression.

The parameters of the peak-selecting program were varied for ten different cases from very restrictive criteria yielding few peaks to non-restrictive criteria giving many more peaks, especially at low temperatures. The final histogram derived from each case showed a progression with very nearly the same energy spacings as in Figure 13, but the heights and detailed shapes of the peaks differed. The parameters that gave the peaks marked in Figures 10-12 were subjectively selected from the ten sets that were used.

The sharp features of the histogram are interpreted as relative spacing of a set of vibrational levels in the upper electronic state. The features of the histogram are listed in Table 1. The first peak is the most abundant; it averages an energy spacing of 500 cm^{-1}; and it presumably includes

cases where two transitions terminate at v' and v' + 1. The second peak is at 980 cm^{-1}, and it presumably includes the pairs of transitions that terminate at v' and v' + 2. The sixth peak is at 2840 cm^{-1}, and it presumably includes the pairs of transitions that terminate in v' and v' + 6. The average spread is 473 cm^{-1}. The trend of E/n from 500 cm^{-1} for the first entry in Table 1 to 473 for the last entry is related to but not identical with the convergence of non-harmonic energy levels in a vibrational spectrum. Each entry in Table 1 includes a family of pairs of transitions. For the first entry in Table 1, the $\Delta\nu'$ would be close to the fundamental frequency at low values of ν', but it would be less than the fundamental frequency due to anharmoncity at high values of ν'. The average of the six values of E/n in Table 1 is 480 cm^{-1}, and the maximum value is 500 cm^{-1}. In view of the experimental error of the method, a fundamental frequency of the excited state is taken to be 480 to 500 cm^{-1}. This frequency is identified as that of the ν_2' bending mode.

The ^{15}N isotope effects. For this discussion, the four isotopic species of nitrous oxide are abbreviated as follows:

$$A = {}^{14}N{}^{14}N{}^{16}O \qquad (3)$$
$$B = {}^{14}N{}^{15}N{}^{16}O$$
$$C = {}^{15}N{}^{14}N{}^{16}O$$
$$D = {}^{15}N{}^{15}N{}^{16}O$$

The frequency ν/cm^{-1} between the first excited level of the ground-state bending mode ν_2'' and the general ν_2' bending vibrational quantum number of the non-linear excited electronic state is

$$\nu = T_e + 1/2\left(\nu_1' + \nu_2' + \nu_3'\right) + \nu_2'\,\nu_2' - \left[1/2\left(\nu_1'' + 2\,\nu_2'' + \nu_3''\right) + \nu_2''\right] \quad (4)$$

where T_e is difference between the bottom of the potential energy wells in the ground and excited electronic states. With the definitions, $Z' = 1/2\left(\nu_1' + \nu_2' + \nu_3'\right)$ and $Z'' = 1/2\left(\nu_1'' + 2\,\nu_2'' + \nu_3''\right)$, (4) may be condensed

$$\nu = T_e + Z' + \nu_2'\,\nu_2' - Z'' - \nu_2'' \quad (5)$$

For a given vibrational transition, the difference in frequency between two isotopic species is

$$\Delta\nu = \Delta Z' - \Delta Z'' - \Delta\nu_2'' + \nu_2'\,\Delta\nu_2' \quad (6)$$

The spectra of the four isotopic species, Figures 3-6, were separated into (000) and (010) components as described above, and the four deconvoluted spectra were pairwise superimposed to give six comparisons, A-B, A-C, A-D, B-C, B-D, C-D. The B-D comparison is given as Figure 14.

At high energies in Figure 14 there is a substantial difference between the two isotopic species, but at low energies the isotope shift and the random experimental error are about equal. For each peak the difference between peak height and the next minimum in the direction of lower energy was found. The isotope shift is defined as the difference in frequency at one-half this relative peak height between two isotopic species. In Figure 14, this isotopic shift was measured for the peaks numbered 1 to 10, where the numbers appear above the peaks. For three out of the six isotopic pairs, A-C, A-D, B-D, this procedure

was used to get a measure of the isotopic shift for these same ten peaks. For the other three cases, the isotope shift could be obtained only for six, six, or three out of ten cases. The observed isotope shifts for these six pairs of observations are given in Table 2. The number sequence, n = 1 to 10, corresponds to the ten numbers written above the peaks in Figure 14. It can be seen in Figure 14 that there are other peaks at energies below n = 1, but the isotopic shift could not be read from these data. Whether the lowest transition, $v_2'(0) \leftarrow v_2''(1)$, is observed or not, there must be some definite number, K, of vibrational levels below the observed peak, n = 1, in Figure 14.

The quantum number for the bending vibrational mode in the upper electronic state may be written: $v_2' = K + n$; and (6) may be re-expressed:

$$\Delta\nu(n) = M + n\,\Delta\nu_2' \qquad (7)$$

where $\Delta\nu(n)$ are the observed shifts as a function of n, Table 2, M is constant for a given isotope pair, and $\Delta\nu_2'$ is the difference in the upper state fundamental bending frequency of the isotope pair. A least-squares fit of $\Delta\nu(n)$ against n gives an estimate of $\Delta\nu_2'$ (which is refined later) for the three cases with ten values of n:

Isotopic species	Estimated $\Delta\nu_2'/cm^{-1}$	(8)
A-C	8.6	
A-D	11.2	
B-D	6.2	
A-B = (A-D) - (B-D)	5.0	

With these three data and the fundamental frequency 490 ± 10 cm^{-1} for ν_2', there are enough observations to make it significant to compare experimental data against a normal-coordinate analysis of the excited state of N_2O.

The first column of Table 3 gives geometrical and dynamic properties of ground-state nitrous oxide.[27,28] The three isotopic shifts for the pairs A-B, A-C, and A-D are included, the other three pairs are not independent, but they may be derived from these three. It is assumed that the bond orders in ground-state nitrous oxide are: 2.5, NN; 1.5, NO; and it is assumed that in the excited state a bonding electron has been excited into an anti-bonding orbital, so that the bond orders are: 2, NN; 1, NO. With this change in bond orders, one uses empirical formulas[31] to evaluate the N-N and N-O bond lengths and stretching force constants, which are entered in the second column in Figure 3. This empirical procedure is not useful for estimating the bending force constant F_ϕ or the bond angle ϕ of the excited state. Normal coordinate calculations[32] were carried out for a wide range of assumed bending force constants F_ϕ and for bond angles at every ten degrees between 90° and 180°. A portion of these calculations is given in Table 4.

The calculated bending frequency ν_2' is plotted against bond angle for various values of the bending force constant in Figure 15. The observed value of the bending frequency are regarded as being between 480 and 500 cm^{-1}, which are indicated as dashed lines on Figure 15. There are many pairs of force constants F_ϕ and bond angles ϕ that give values of ν_2' in agreement with experiment. The isotopic shifts $\Delta\nu_2'$ were calculated as a function of bond angle and for ν_2' = 480 cm^{-1} and for ν_2' = 500 cm^{-1}, cutting across various values of bending force constants;

and these calculated isotope shifts are the three pairs of lines in Figure 16. The method of deriving the range of observed isotope shifts is given below.

The zero-point energy, $\Delta Z'$, was evaluated for all cases in Table 4. It was found that $\Delta Z'$ changed very slowly with ϕ and F_ϕ, and any changes are negligible over the range of conditions that yield $\nu_2' = 490 \pm 10$ cm^{-1}. Thus within the framework of this model and these observations, $\Delta Z'$ as well as $\Delta Z''$ and ν_2'' are known. The quantity K, which locates the origin of ν_2', may be estimated from the intercept of the least-squares fit of $\Delta\nu(n)$ vs $\underline{n}$ (6):

$$K = \left[\Delta\nu(n) + \Delta Z'' + \nu_2'' - \Delta Z'\right]_{n=o} / \Delta\nu_2' \qquad (9)$$

For the three cases with ten values of $\underline{n}$ in Table 2, the intercepts at $\underline{n} = 0$ were:

$$\begin{aligned} &\text{A-C, } K = 4.2 \\ &\text{A-D, } K = 4.6 \\ &\text{B-D, } K + 5.6 \end{aligned} \qquad (10)$$

The average of these values is 4.8, and since K must be an integer this value was rounded to 5. With this value of K, each entry in Table 2 gives an estimate of the corresponding value of $\Delta\nu_2'$ from the expression

$$\Delta\nu_2' = \left(\Delta\nu(n) + \Delta Z'' + \Delta\nu_2'' - \Delta Z'\right)/(5 + n) \qquad (11)$$

These values are entered in Table 5, along with $\Delta\Delta Z = \Delta Z'' - \Delta Z'$. For a given isotopic pair the estimated isotope shift $\Delta\nu_2'$ is reasonably uniform with n.

The average values of $\Delta\nu_2'$ over the peaks $\underline{n}$ and twice the standard deviation are entered as the "direct" estimation of the six pairs of isotopes in Table 6. Of these six pairs there are only three independent pairs, which may be taken to be A-B, A-C, and A-D. However, there is, unavoidably, some subjectivity in reading the isotope shifts from the data, such as Figure 14, and it is desirable to use all of the data and all six comparison in estimating the three independent pairs. The difference A-B may be estimated in four ways:

$$(A-B) \qquad (12)$$

$$(A-C) - (B-C)$$

$$(A-D) - (B-D)$$

$$(A-D) - (C-D) - (B-C)$$

Similarly (A-C) or (A-D) may be measured directly and derived from three other relations. For each of the three independent pairs, the direct and derived estimates of isotope shifts are included in Table 6. The average of the four estimates and twice the standard deviation for each of the three isotope shifts are given as the last column in Table 6. These three values and their estimated precision are regarded as "observed quantities" and entered as such in Table 7b, and plotted as the dashed horizontal lines in Figure 16. If the excited state is linear, the isotope shifts should increase in the order, A-C, A-B, A-D; if the excited state has a 90° bond angle, the order is A-B, A-C, A-D; and the cross-over between these two sequencies occurs at an angle of about 135°. The observed order is A-B, A-C, A-D, which confirms that the excited state is non-linear. Within the estimated error range of ν_2', 490 ± 10 cm^{-1} and of the isotope shifts (Table 6), the overlap

between calculated and observed quantities in Figure 16 indicates a bond angle between 110° and 120°.

For $F_\phi/10^{-12}$ = 7, 8, 9 and 10, the values of ν_2' at 480, 490, and 500 cm^{-1} were interpolated from Table 4 and entered in Table 7a along with the other calculated quantities: bond angle, ϕ; frequencies, ν_1' and ν_3'; and isotope shifts, A-B, A-C, and A-D. At each frequency, 480, 490, or 500, and force constant F_ϕ, the sum of the squares $\left(\Delta\nu'_{CALC} - \Delta\nu'_{OBS}\right)^2$ was calculated and plotted against force constant. The force constant that gave minimum sum-of-squares deviation is entered for each frequency in Table 7c, and all other terms were interpolated to this force constant. The three rows of Table 7c give the range of calculated quantities that best agree with the four observations (Table 7b) of this study. At the central frequency, 490 cm^{-1}, the calculated isotope shifts and observed isotope shifts agree within the precision of the observed isotope shifts: 4.1 relative to 4.5 ± 0.7; 6.8 relative to 7.5 ± 0.7; and 10.8 relative to 11.1 ± 0.6. The agreement between observation and model is slightly better if ν_2' is 500 cm^{-1} and slightly worse if ν_2' is 480 cm^{-1}. The bond angle is estimated to be 114 to 115°; the calculated ν_1' stretch frequency is 1368 to 1375; and the range of calculated ν_3' stretch is 1759 to 1763. The range of bending force constants is 8.3 to 9.1 x 10^{-12} erg rad^{-1}.

The structural and vibrational properties of the excited electronic state are compared with those of the ground electronic state in Table 3. The first four quantities in the last column are the assumed input to the model; the last eight quantities are determined by the observed isotope shifts and the model. Although linear in the ground electronic state, nitrous oxide is bent with 115° bond angle in the excited electronic

state. The bending frequency is 589 cm^{-1} in the ground state and somewhat lower at 490 ± 10 cm^{-1} in the excited state. The ν_1 frequency is somewhat higher and the ν_3 frequency is lower in the excited electronic state; the sum of the two stretching frequencies is 3133 cm^{-1} for the excited state and 3509 cm^{-1} in the ground state. The bending force constant appears to be larger in the excited state, 8.7 vs 6.9 x 10^{-12} erg rad^{-1}. The order of the ν_2 isotope shift for the sequence A-B, A-C, and A-D is different in the excited state and ground state, which is itself strong evidence that the excited state is non-linear (compare Figure 16).

The isotopic data indicate that the origin of the progression is 6 vibrational quanta below the peak labeled n = 1 in Figure 14 at 53050 cm^{-1}. The resultant origin of the progression is about 50100 cm^{-1} or 6.21 eV. The energy separation between the minima of the two potential wells, T_e, would be 51230 cm^{-1} or 6.35 eV and the energy separation of the two (000) levels is 50700 cm^{-1} or 6.29 eV. The observed peaks extend from $v_2' = 2$ to 15 and originate primarily from $v_2'' = 1$. The transition to $v_2' = 1$ cannot be resolved and $v_2' = 0$ is off-scale at low energies. The vibrational progression from (000) to $(v_2' - 1)$ would be 100 cm^{-1} higher in energy than the stronger transition of (010) to v_2' and this may contribute to the broadness of the bands.

Interpretation of the Observed Transitions

There have been several calculations of vertical excitation energies of the lower lying electronic states of nitrous oxide.[34-39] Below 9.5 eV there is agreement on the presence of seven excited electronic states. Table 8 lists these states, their vertical excitation energies and

their asymptotic energies for each possible mode of photodissociation. While for each state there is a degree of uncertainty in the calculated vertical excitation energy, there is good agreement between the results of calculation of the same type. The two CI and MCSCF calculations agree well; of these the results of Winter[35] and Fortune[37] are preferred as they used a larger basis set than that of Peyerimhoff.[34] Agreement is also observed for the semi-empirical HF, INDO and SCF calculations, but the more extensive CI calculations are generally preferred over these. The semi-empirical HAM/3 calculation gives values between these two sets.

Structured absorption. Of the electronic states available at energies less than 9.5 eV, only the $^3\Sigma^+$, $^3\Delta$ and $^1\Sigma^-$ states are calculated to be bound relative to their asymptotic energies. Absorption into the triplet states is optically forbidden from the singlet ground state. $^1\Sigma^- \leftarrow \tilde{X}^1\Sigma^+$ is symmetry forbidden as an electric dipole transition but is allowed as a magnetic dipole transition. The $^1\Sigma^-$ state has been calculated to be bent in its equilibrium geometry with a bond angle of 129°.[37] The bond angle of 115° determined in this study is reasonably close to the calculated value, however a recalculation of the equilibrium bond angle would be useful since the Fortune study did not optimize bond lengths in their calculation of bond angle.

Assignment of the structured absorption observed between 6.3 and 7.3 eV to the $^1\Sigma^- - \tilde{X}$ transition may explain the important role of the vibrational bending mode in the optical absorption. Vertical transitions from the ground electronic state excited in the bending vibration would result in a nonlinear configuration of the upper state. For an

upper state with a nonlinear equilibrium geometry, a transition from a bent lower state would have favorable Franck-Condon overlap. Enhanced oscillator strength of this transition would also result from the reduced symmetry of the two states. The equivalent transition in C_s symmetry, $^1A''(^1\Sigma^-) \leftarrow \tilde{X}^1A'(\tilde{X}^1\Sigma^+)$ is allowed. This is in agreement with the experimental observation of a defined structured absorption by molecules in the (010) vibrational mode. The $^3\Sigma^+$ and $^3\Delta$ bound states would also have reduced symmetry upon bending, but would remain as forbidden triplet-singlet transitions. Vertical transitions from a linear ground state would result in a linear configuration in the upper state and be weak as the $^1\Sigma^- - {}^1\Sigma^+$ transition is symmetry forbidden. The very weak structuring found in the absorption spectrum of molecules in the (000) mode is $\sim$ 4% of the intensity of structuring observed in the (010) absorption spectrum.[42] This weak structuring may contain a magnetic dipole contribution as the observed intensity is consistent with the expected intensity for an allowed magnetic dipole transition.[40]

The results of the CI calculations listed in Table 8 lend support to this assignement for the structured absorption. The energy range of banding between 6.3 and 7.3 eV agrees well with the calculated vertical energy for the bound $^1\Sigma^-$ state while $^3\Delta$ and $^3\Sigma^+$ are calculated at lower levels. Results from the vacuum spectrograph show the structured absorption to drop off, or show an edge above 7.3 eV. Above this energy the $^1\Sigma^-$ state is not bound in N-NO dimension. This assignment is also in agreement with the electron impact spectra of Hall.[33] Based upon the residual energy dependence of a feature he observed at $\sim$ 6.2 eV, he determined the transition to be spin allowed and assigned it as $^1\Sigma^- - \tilde{X}$.

Continuous absorption. An apparent continuous absorption is observed at all temperatures underlying the structured absorption. This continuous absorption has been well noted in the literature and will only be discussed briefly. The repulsive state responsible for this absorption is generally believed to be $^1\Delta$[10,11,35-38,44] accounting for its relatively weak intensity. The role of the ν_2" bending vibration in the temperature dependence of the continuous absorption has been interpreted to some extent using Herzberg-Teller theory.[41] The $^1\Delta$ assignment appears reasonable as it is repulsive along the N_2-O hypersurface correlating adiabatically with $N_2(\tilde{X}) + O(^1D)$ with an asymptotic energy of 3.65 eV. Experimentally, the continuous absorption reaches a maximum at 6.85 eV and extends weakly to $\sim$ 4.7 eV.[22] There is considerable evidence that photodissociation over this wavelength range gives N_2 + $O(^1D)$ as its sole product. The only other repulsive states in this energy range, $^3\Sigma^-$ and $^3\pi$, are triplet-singlet transitions that correlate adiabatically with $N_2(\tilde{X}) + O(^3P)$. The $^1\pi$ state is calculated to lie at higher energies and is thought responsible for the more intense absorption of nitrous oxide at 8.7 eV.[10,36,44]

Predissociation of $^1\Sigma^-$. The model of the absorption process presented here, a composite of a structured absorption, $^1\Sigma^- - \tilde{X}$, and a continuous absorption, $^1\Delta \leftarrow \tilde{X}$, places the two electronic states at nearby energies. This is verified in Table 8 where it is seen that each calculation places the two states within 0.3 eV of each other in their vertical excitation energies. The $^1\Sigma^-$ and $^1\Delta$ states have both been calculated to be bent in their equilibrium geometry with differing bond

angles[37] and thus it is possible that at a given bond angle the N_2-O hypersurfaces of the bound and repulsive states may cross. At this point of crossing, mixing of the two states may be expected to take place. This is due to the intersection of a $^1A''$ component in C_s symmetry of $^1\Delta$ with the $^1A''$ curve correlating with $^1\Sigma^-$. The resultant avoided crossing between the $^1\Sigma^-$ and $^1\Delta$ states may provide a pathway for predissociation of the bound state along the N_2-O surface. A similar situation for HNO has been discussed in detail by Herzberg and Longuet-Higgins.[43] In this case, the $^1\pi$ and $^1\Delta$ states each form a $^1A'$ and $^1A''$ component upon bending. The $^1A'$ state can intersect the $^1A''$ state, but an avoided crossing results when states of the same C_s symmetry intersect.

Acknowledgment

The authors wish to express their gratitude to Sumner P. Davis and John Conway of the Lawrence Berkeley Laboratory for the use of their 3 m vacuum spectrograph.

This work was supported by the Division of Chemical Sciences, Office of Basic Energy Sciences, U.S. Department of Energy under Contract No. W-7405-Eng-48.

References

1. Leifson, S. W., Astrosphys. J., 63, 73 (1926).
2. Dutta, A. K., Proc. Roy. Soc. (London), 138, 84 (1932).
3. Sponer, H. and L. G. Bonner, J. Chem. Phys., 8, 33 (1940).
4. Holliday, M. G. and B. G. Reuben, Far. Soc. Trans., 64, 1735 (1968).
5. Nicolle, J. and B. Vodar, Compt. Rend., 210, 142 (1940).
6. Thompson, B. A., P. Harteck and R. R. Reeves, J. Geophys. Res., 68, 6431 (1963).
7. Duncan, A. B. F., J. Chem. Phys., 4, 638 (1936).
8. Romand, J. and J. Mayence, Compt. Rend., 228, 998 (1949).
9. Zelikoff, M., K. Watanabe and E. C. Y. Inn, J. Chem. Phys., 21, 1643 (1953).
10. Rabalais, J. W., J. M. McDonald, V. Scherr and S. P. McGlynn, Chem. Revs., 71, 73 (1971).
11. Monahan, K. M. and W. C. Walker, J. Chem. Phys., 63, 1676 (1975).
12. Wulf, O. R. and E. H. Melvin, Phys. Rev., 39, 180 (1932).
13. Sen-Gupta, P. K., Nature, 136, 513 (1935).
14. Henry, L., Nature, 134, 498 (1934).
15. Doering, J. P. and B. H. Mahan, J. Chem. Phys., 36, 1682 (1962).
16. Yamazaki, H. and R. J. Cvetanovic, J. Chem. Phys., 41, 3703 (1964).
17. Paraskevopoulos, G. and R. J. Cvetenovic, J. Am. Chem. Soc., 91, 7572 (1969).
18. Paraskevopoulos, G. and R. J. Cvetanovic, J. Chem. Phys. 52, 5821 (1970).
19. Preston, K. F. and R. F. Barr, J. Chem. Phys., 54, 3347 (1971).
20. Simonaitis, R., R. I. Greenberg and J. Heicklen, Int. J. Chem. Kin., 4, 497 (1972).

21. Bates, D. R. and P. B. Hays, Planet. Space Sci., 15, 189 (1967).

22. Johnston, H. S. and G. S. Selwyn, Geophys. Res. Lett., 2, 549 (1975).

23. Lassettre, E. N., A. Skerbele, M. A. Dillon and K. J. Ross, J. Chem. Phys., 48, 5066 (1968).

24. Selwyn, G. S., J. Podolske and H. S. Johnston, Geophys. Res. Lett., 4, 427 (1977).

25. Ackerman, M. and F. Biaume, J. Mol. Spect., 35, 73 (1970).

26. Coleman, C. D., W. R. Bozeman and N. F. Maggers, Table of Wavenumbers, Nat. Bur. Stand. Monograph 3, U.S. Govt. Print. Off., Washington, D.C. (1960).

27. Pliva, J., J. Mol. Spectroscopy, 12, 360 (1961) and redetermination in this study.

28. Herzberg, G., Infrared and Raman Spectra, Vol. II, Van Nostrand Reinhold, New York, 1945, p 174.

29. See for example, McQuarrie, D. A., Statistical Mechanics, Harper and Row, New York, 1976, p 130.

30. Herzberg, G., Elect. Spectra and Elect. Struct. of Poly. Mol., Vol. III, Van Nostrand Reinhold, New York, 1966, pp 451-453.

31. Johnston, H. S., Gas Phase Reaction Rate Theory, The Ronald Press Co., New York, 1966, pp 81-82.

32. Wilson, E. B., Jr., J. C. Decius and P. C. Cross, Molecular Vibrations, McGraw-Hill Book Company Inc., New York, 1955.

33. Hall, R. I., A. Chutjian and S. Trajmar, J. Phys. B.: At. Mol. Phys., 6, L365 (1973).

34. Peyerimhoff, S. D. and R. J. Buenker, J. Chem. Phys., 49, 2473 (1968).

35. Winter, N. W., Chem. Phys. Lett., 33, 300 (1975).

36. Krauss, M., D. G. Hopper, P. J. Fortune, A. C. Wahl and T. O. Tiernan, ARL TR-75-0202, Vol. 1, Air Force Systems Command (1975). Available from Natl. Tech. Info. Serv., U.S. Dept. of Commerce, Springfield, Virginia 22151.

37. Fortune, P. J., D. G. Hopper, B. J. Rosenberg, W. B. England, G. Das, A. C. Wahl and T. O. Tiernan, ARL TR-75-0202, Vol. 2, Air Force Systems Command (1975). Available from Natl. Tech. Info. Serv., U.S. Dept. of Commerce, Springfield, Virginia 22151.

38. Frindh, C., L. Asbrink and E. Lindholm, Chem. Phys., 27, 169 (1978). Values listed were read from Figure 4.

39. Chutjian, A. and G. A. Segal, J. Chem. Phys., 57, 3069 (1972).

40. See pp 134-135 of Reference 30.

41. Innes, K. K., J. Mol. Spect., 42, 575 (1972).

42. The intensity of structuring is measured peak to trough, and so lack of resolution in the pronounced structuring of (010) mode may further increase the difference of structuring intensity between the (000) and (010) vibrational modes.

43. Herzberg, G. and H. C. Longuet-Higgins, Disc. Far. Soc., 35, 77 (1963).

44. Huebner, R. H., R. J. Celotta, S. R. Mielczarek and C. E. Kyatt, J. Chem. Phys., 63, 4490 (1975).

45. Selwyn, G. S., Ph.D. Thesis, University of California, Berkeley, 1979.

Table 1. Vibrational features and energy levels obtained from the histogram of Figure 13.

Relative Vibrational Level	Energy, cm^{-1}	E/n, cm^{-1}
1	500	500
2	980	490
3	1420	473
4	1880	470
5	2340	468
6	2840	473
		Average 479

Table 2. Observed isotope shifts, $\Delta\nu_2'(n)/cm^{-1}$, between various pairs of species.

Species*	Differences in frequency, cm^{-1}									
n	1	2	3	4	5	6	7	8	9	10
A-B					26	31	37	41	47	52
A-C	37	43	50	57	73	80	87	94	105	112
A-D	35	40	54	64	77	89	98	109	123	133
B-C					44	45	46	54	59	65
B-D	33	37	45	50	59	64	65	76	83	89
C-D								18	24	30

*A, NNO; B, $N^{15}NO$; C, ^{15}NNO; D, $^{15}N^{15}NO$.

Table 3. Ground state and excited state properties of nitrous oxide ($^{14}N^{14}N^{16}O$).

	Ground State	Ref.	Excited State
$R_{NN}/10^{-8}$ cm	1.15	28	1.18[a]
$R_{NO}/10^{-8}$ cm	1.23	28	1.29[a]
$F_{NN}/10^{5}$ dynes cm^{-1}	14.6	28	11.7[b]
$F_{NO}/10^{5}$ dynes cm^{-1}	13.7	28	9.13[b]
ϕ/degrees	180	28	114 to 115[b]
$F_{\phi}/10^{-12}$ ergs rad^{-1}	6.9	28	8.7 ± 0.4[b]
ν_1/cm^{-1}	1285	28	1372 ± 4[b]
ν_2/cm^{-1}	589	28	490 ± 10[c]
ν_3/cm^{-1}	2224	28	1761 ±2[b]
$\Delta\nu_2$(14,14,16)-(14,15,16)	13.5	27	4.5 ± 0.7[c]
$\Delta\nu_2$(14,14,16)-(15,14,16)	3.5	27	7.5 ± 0.7[c]
$\Delta\nu_2$(14,14,16)-(15,15,16)	16.9	27	11.1 ± 0.6[c]

[a]Derived from change in bond order, resulting from ($2\pi \rightarrow \pi^*$) transition.

[b]Calculated value using experimental and derived values as input, see text.

[c]Experimental value.

Table 4. Calculated frequencies and isotopic frequency shifts for the bending vibrations of electronically excited N_2O.

$F/10^{-12}$ ergs rad	ϕ deg.	ν_{2A}/cm^{-1}			$\Delta\nu_2/cm^{-1}$		
		ν_1'	ν_2'	ν_3'	(A-B)	(A-C)	(A-D)
10	90	1456	467	1693	2.1	7.5	9.5
	100	1446	488*	1705	2.8	7.5	10.2
	110	1403	512	1741	3.7	7.4	11.0
	120	1347	538	1785	4.9	7.2	12.1
9	90	1455	444	1692	2.0	7.1	9.1
	100	1443	464	1704	2.8	7.1	9.8
	110	1400	487*	1740	3.6	7.0	10.6
	120	1342	512	1785	4.8	6.8	11.6
	130	1280	539	1828	6.2	6.6	12.7
	140	1218	568	1865	8.0	6.2	14.1
	150	1160	597	1897	10.0	5.7	15.6
	160	1113	623	1919	12.2	5.0	17.2
	170	1081	642	1933	14.1	4.3	18.5
	180	1070	649	1938	14.9	4.0	19.0
8	110	1396	460	1740	3.5	6.6	10.0
	120	1338	484*	1784	4.6	6.4	11.0
	130	1276	510	1828	6.0	6.2	12.1
	140	1214	537	1866	7.7	5.8	13.4
7	120	1335	454	1784	4.5	6.0	10.4
	130	1272	478*	1828	5.8	5.7	11.4
	140	1211	504	1866	7.4	5.4	12.7
	150	1155	529	1896	9.2	4.8	14.0
6	130	1268	444	1827	5.5	5.2	10.7
	140	1207	468	1866	7.0	4.9	11.8
	150	1153	491*	1897	8.7	4.4	13.1
	160	1109	511	1919	10.3	3.9	14.2

*ν_2' is within range 490 ± 10 cm^{-1}, the observed value.

Table 5. Values of isotope shift, $\Delta\nu_2'/cm^{-1}$, deduced from observed $\Delta\nu(n)$ and calculated differences in zero point energies, $\Delta Z/cm^{-1}$. Equation (11).

Species*	$\Delta\Delta Z/cm^{-1}$	Vibrational quantum number, ν_2'									
		6	7	8	9	10	11	12	13	14	15
A-B	22.3					4.8	4.8	4.9	4.9	5.0	5.0
A-C	7.6	7.4	7.2	7.2	7.2	8.1	8.0	7.9	7.8	8.0	8.0
A-D	31.1	11.0	10.2	10.5	10.6	10.8	10.9	10.8	10.8	11.0	10.9
B-C	-14.7					2.9	2.9	2.6	3.0	3.2	3.4
B-D	8.8	7.0	6.5	6.7	6.5	6.8	6.6	6.2	6.5	6.6	6.5
C-D	23.5								3.2	3.4	3.6

*A, NNO; B, $N^{15}NO$; C, ^{15}NNO; D, $^{15}N^{15}NO$.

Table 6. Values of isotope shift, $\Delta\nu_2'/cm^{-1}$, as averages of all data in Table 1.

	Direct		Derived		Average
A-B	4.9 ± 0.2	4.7	4.2	4.4	4.5 ± 0.7
A-C	7.7 ± 0.8	7.9	7.3	7.1	7.5 ± 0.7
A-D	10.8 ± 0.5	11.5	11.1	11.3	11.1 ± 0.6
B-C	3.0 ± 0.6				
B-D	6.6 ± 0.4				
C-D	3.4 ± 0.4				

Table 7. Observed quantities and interpolated values of calculated frequencies and isotope shifts.

$F/10^{-12}$ ergs rad.	ϕ deg.	ν_A'/cm^{-1}			$\Delta\nu'/cm^{-1}$		
		ν_1'	ν_2'	ν_3'	(A-B)	(A-C)	(A-D)
(a) Calculated quantities interpolated to selected values of ν_2'.							
10	96	1450	480	1700	2.6	7.5	10.0
9	107	1413	480	1729	3.4	7.0	10.3
8	118	1348	480	1777	4.5	6.4	10.8
7	131	1267	480	1831	5.9	5.7	11.5
10	101	1442	490	1708	2.9	7.4	10.3
9	111	1392	490	1746	3.8	7.0	10.7
8	122	1324	490	1794	5.0	6.4	11.2
7	134	1244	490	1845	6.5	5.6	12.0
10	105	1424	500	1723	3.3	7.4	10.6
9	115	1370	500	1763	4.2	6.9	11.1
8	126	1300	500	1811	5.5	6.3	11.7
7	138	1220	500	1860	7.1	5.4	12.5
(b) Observed quantities.							
			490 ± 10		4.5	7.5	11.1
					±.7	±.7	±.6
(c) Minimum least-squares deviation of isotope shifts.							
8.3	115	1368	480	1763	4.1	6.6	10.6
8.7	114	1372	490	1760	4.1	6.8	10.8
9.1	114	1375	500	1759	4.1	7.0	11.0

Table 8. Excited electronic states of nitrous oxide with vertical excitation energies of 9.5 eV or less.

State	Winter(35)		Chutjian(39)	Fridh(38)	Peyerimhoff(34)	Fortune(37)		Asymptotic Energy(36)	
	HF	CI	INDO	HAM/3	CI	SCF	MCSCF	N_2-O[a]	NO-N[b]
$\tilde{X}^1\Sigma^+$	0	0	0	0	0	0	0	3.65	7.31
$^3\Sigma^+$	4.0	5.39	3.5	5.3	5.76	3.97	5.32	9.03	7.31
$^3\Delta$	4.5	6.02	4.0	5.7	6.36	4.48	5.91	9.03	7.31
$^3\Sigma^-$	4.9	6.53	4.1	-	6.82	4.89	6.62	1.68	7.31
$^1\Delta$	5.1	6.84	4.3	6.5	7.13	5.09	6.97	3.65	7.31
$^1\Sigma^-$	4.9	6.58	4.2	6.2	6.91	4.89	6.75	7.85	7.31
$^3\pi$	7.5	-	6.1	-	-	7.34	-	1.68	4.93
$^1\pi$	7.7	-	7.0	-	-	7.57	9.3	3.65	7.31

All energies in eV relative to $\tilde{X}^1\Sigma^+$

[a] 1.68, 3.65, 7.85 and 9.03 eV asymptotic energies are respectively $N_2(^1\Sigma_g^+) + O(^3P)$, $N_2(^1\Sigma_g^+) + O(^1D)$, $N_2(^3\Sigma_u^+) + O(^3P)$ and $N_2(^3\pi_g) + O(^3P)$.

[b] 4.93 and 7.31 eV asymptotic energies are respectively $N(^4S) + NO(^2\pi)$ and $N(^2D) + NO(^2\pi)$.

Figure Captions

Figure 1. Schematic design of silica, temperature-controlled, optical cell.

Figure 2. Nitrous oxide absorption cross sections at temperatures (from bottom to top): 151, 182, 196, 223, 243, 268, 301, 333, 372, 423, and 485 K. Wavelength range 172-190 nm. These curves are direct print-out of 900 observed data points.

Figure 3. Absorption cross sections for A = $^{14}N^{14}N^{16}O$ at temperatures 148, 213, 301, 372, 442, and 503 K. Wavelength range 173 to 197 nm. Direct print-out of 1200 observed data points.

Figure 4. Absorption cross sections for B = $^{14}N^{15}N^{16}O$ at temperatures 148, 213, 301, 372, 442, and 503 K. Wavelength range 173 to 197 nm. Direct print-out of 1200 observed data points.

Figure 5. Absorption cross sections for C = $^{15}N^{14}N^{16}O$ at temperatures 148, 213, 301, 372, 442, and 503 K. Wavelength range 173 to 197 nm. Direct print-out of 1200 observed data points.

Figure 6. Absorption cross sections for D = $^{15}N^{15}N^{16}O$ at temperatures 148, 213, 301, 372, 442, and 503 K. Wavelength range 173 to 197 nm. Direct print-out of 1200 observed data points.

Figure 7. Deconvolution of data from Figure 2 at 151 K and 333 K into absorption spectra for (000) and (010) nitrous oxide.

Figure 8. Observed (thin line) and predicted (heavy line constructed from 1024 small circles) spectra at 151, 196, 243, 301, 372, and 485 K from the (000) and (010) spectra as shown in Figure 7. The lowest curve at 151 K was used in fitting the (000) and (010) spectra and it is not "predicted."

Figure 9. Enlargement of vertical scaling shows weak structuring of the 151 K spectrum (dotted line), the (000) mode spectrum (solid line), and the smooth energy-weighted Gaussian curve.

Figure 10. Difference spectrum between observed spectrum at 151 K and the energy weighted Gaussian of Figure 9. The lines mark the peaks selected by the "peak selecting" computer program.

Figure 11. Difference spectrum between that observed at 333 K and an energy-weighted Gaussian, which was fitted below the valleys of the observed data at 333 K. The lines are as described in Figure 10.

Figure 12. Difference spectrum between that observed at 485 K and an energy-weighted Gaussian, which was fitted below the valleys of the observed data at 485 K. The lines are as described in Figure 10.

Figure 13. Histogram of frequency of occurrence of a given energy separation between peaks plotted against energy. The energy lines are 20 cm^{-1} wide. All data at all temperatures are pooled in this figure.

Figure 14. The (000) and (010) spectra for B = $^{14}N^{15}N^{16}O$ and D = $^{15}N^{15}N^{16}O$ as deduced from (1) and Figures 4 and 6. The numbers n = 1 to 10 above the (010) curves correspond to the peaks for which the isotopic difference, $\Delta\nu_2'$, could be obtained. The corresponding differences are entered in Table 2.

Figure 15. Calculated bending frequency ν_2' as a function of bond angle and bending force constants (in units of 10^{-12} $ergs/rad^2$). The horizontal dashed line represents the uncertainty range of observed frequency.

Figure 16. The pairs of solid lines are the calculated isotope shifts (spanning ν_2' = 480 to 500 cm^{-1}) as a function of bond angle (compare Figure 15). The pairs of dashed lines give the estimated uncertainty range of the observed isotope shifts. The three sets of data overlap the calculated lines only for angles between 110° and 120°.

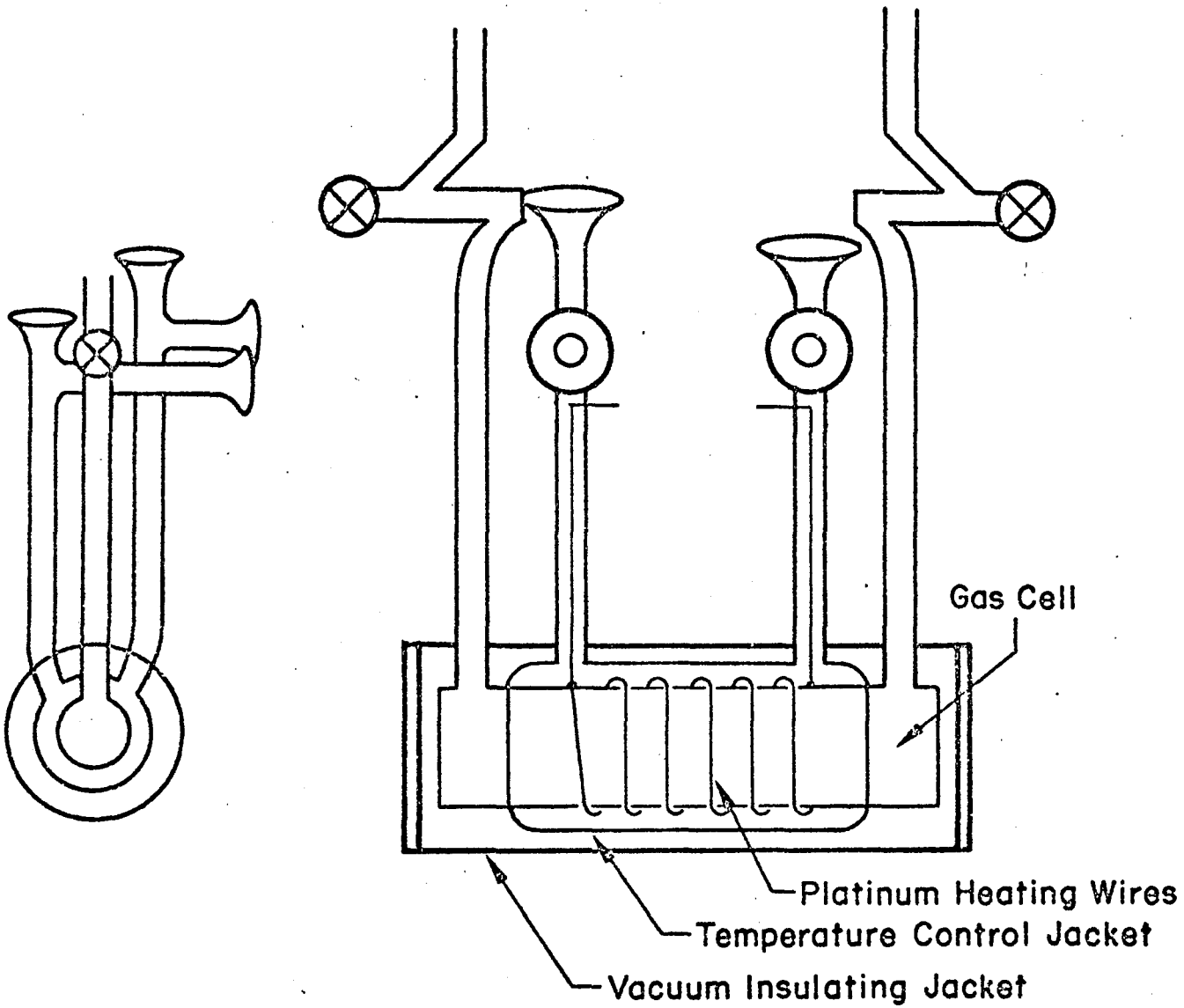
Gas Cell
Platinum Heating Wires
Temperature Control Jacket
Vacuum Insulating Jacket

XBL 792-8344

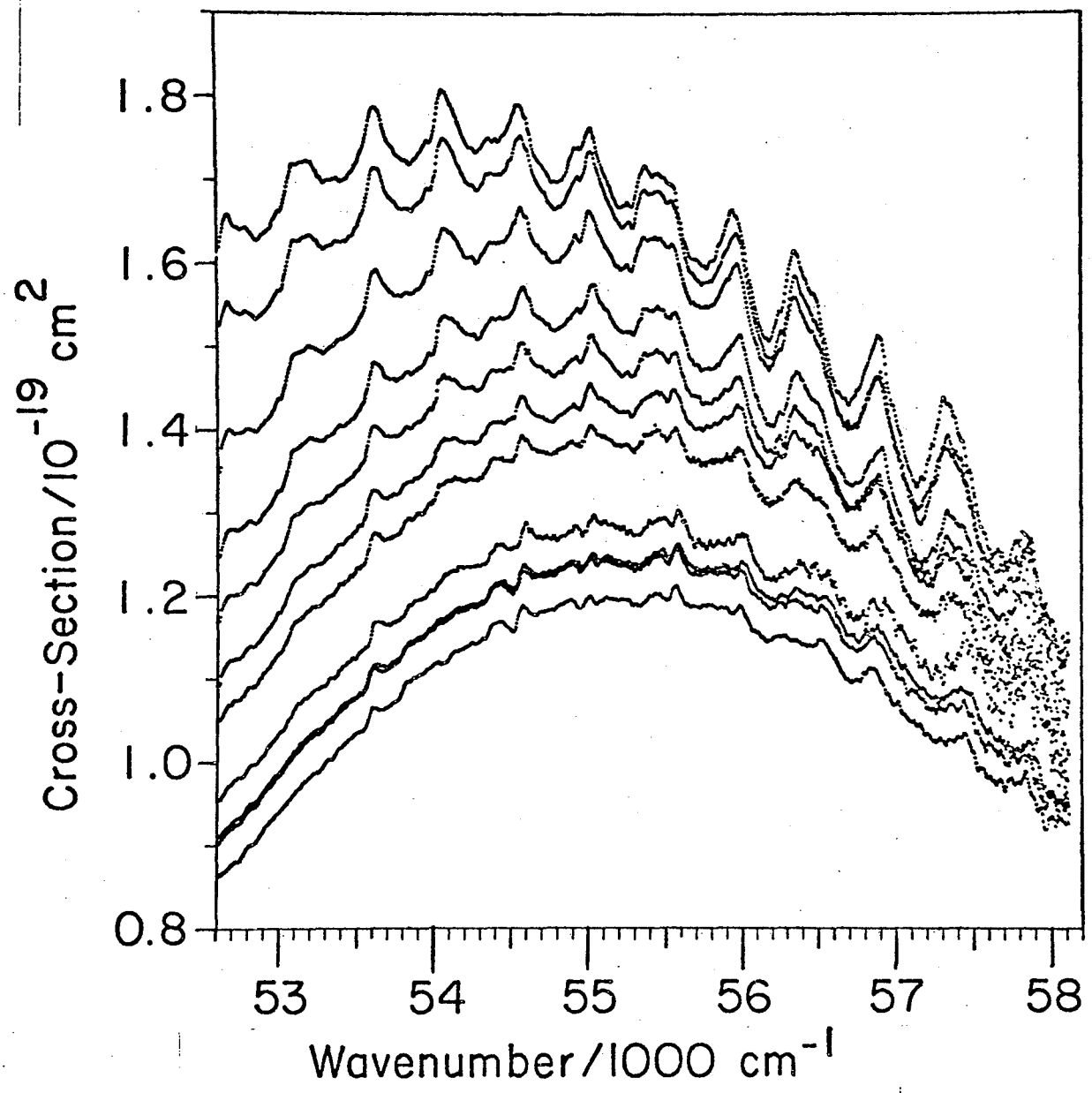
1.8
1.6
1.4
1.2
1.0
0.8
Cross-Section/10^{-19} cm^2
53
54
55
56
57
58
Wavenumber/1000 cm^{-1}

(2)

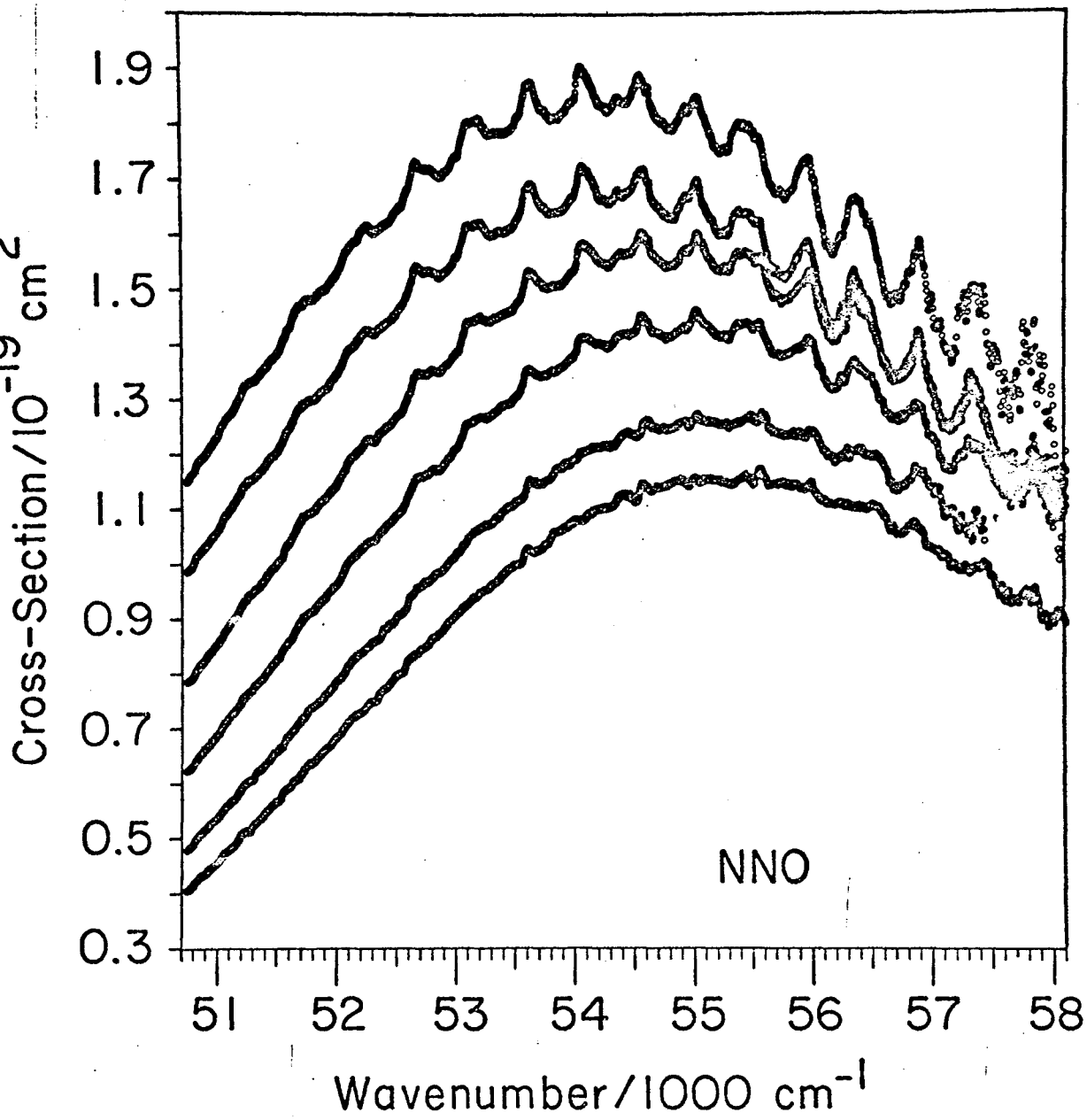
1.9
1.7
1.5
1.3
1.1
0.9
0.7
0.5
0.3
Cross-Section/10^{-19} cm^2
NNO
51
52
53
54
55
56
57
58
Wavenumber/1000 cm^{-1}

(3)

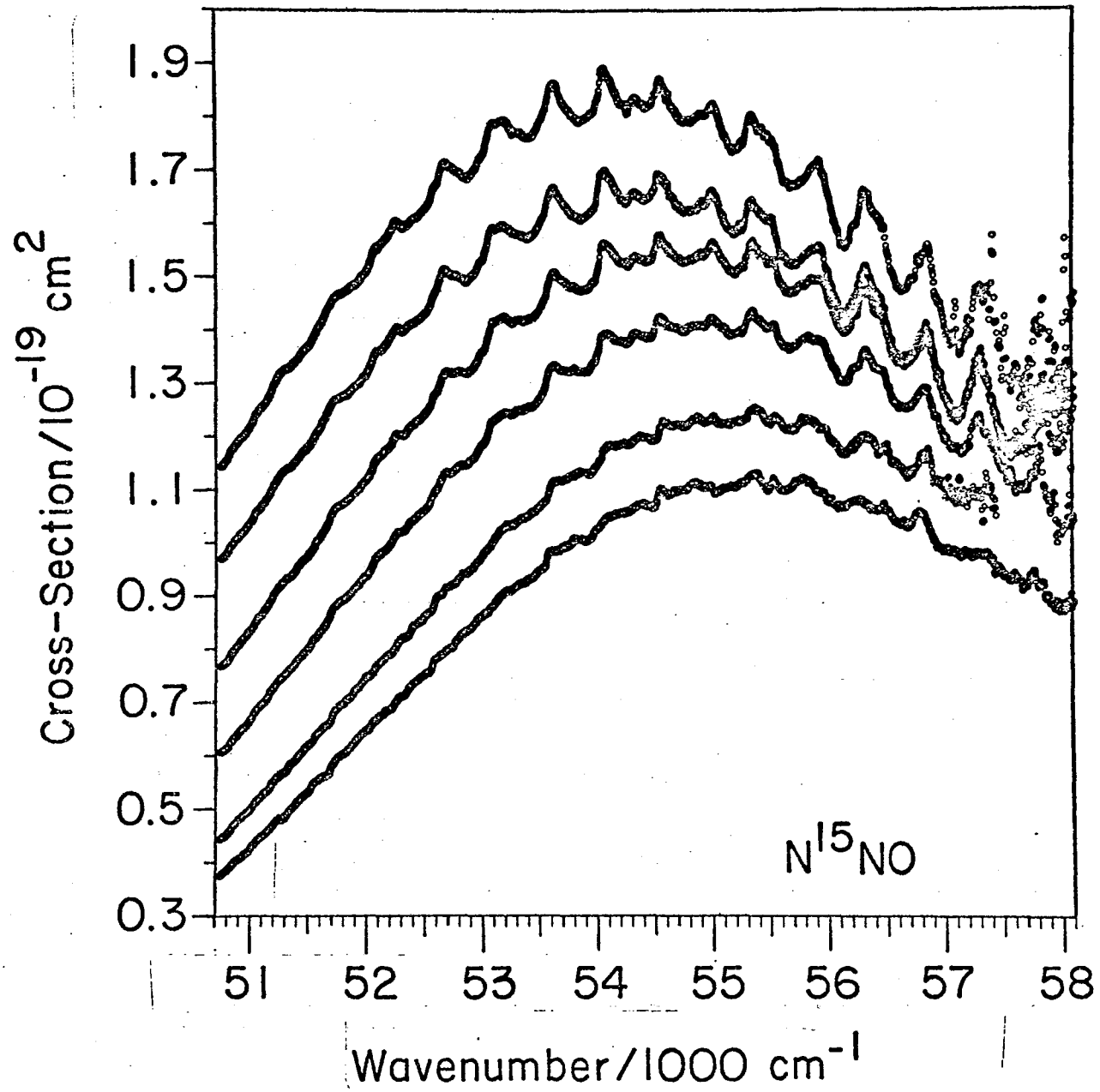
1.9
1.7
1.5
1.3
1.1
0.9
0.7
0.5
0.3
Cross-Section/10^{-19} cm^2
$N^{15}NO$
51
52
53
54
55
56
57
58
Wavenumber/1000 cm^{-1}

(4)

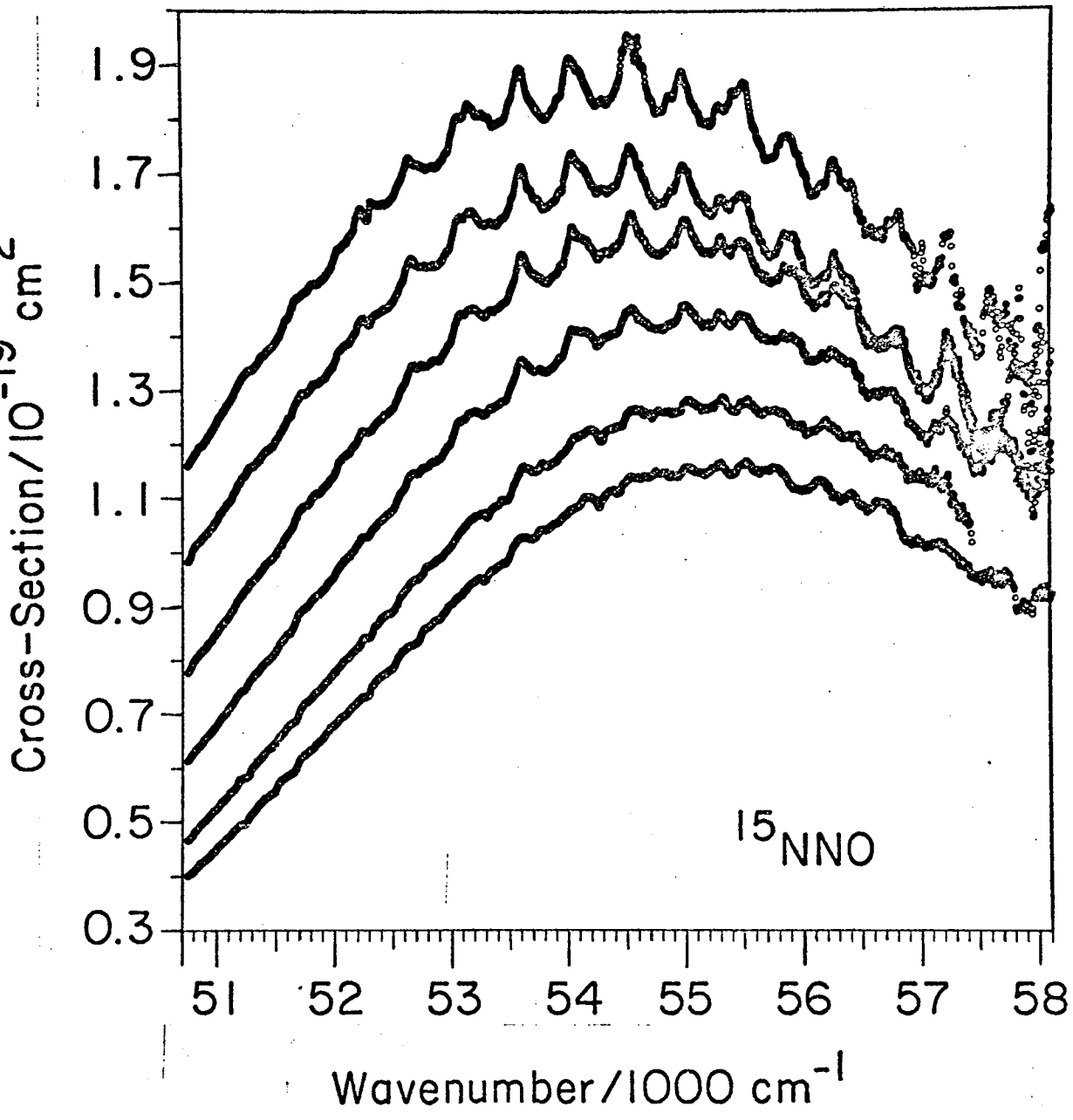
Cross-Section/10^{-19} cm^2
1.9
1.7
1.5
1.3
1.1
0.9
0.7
0.5
0.3
^{15}NNO
51
52
53
54
55
56
57
58
Wavenumber/1000 cm^{-1}

(5)

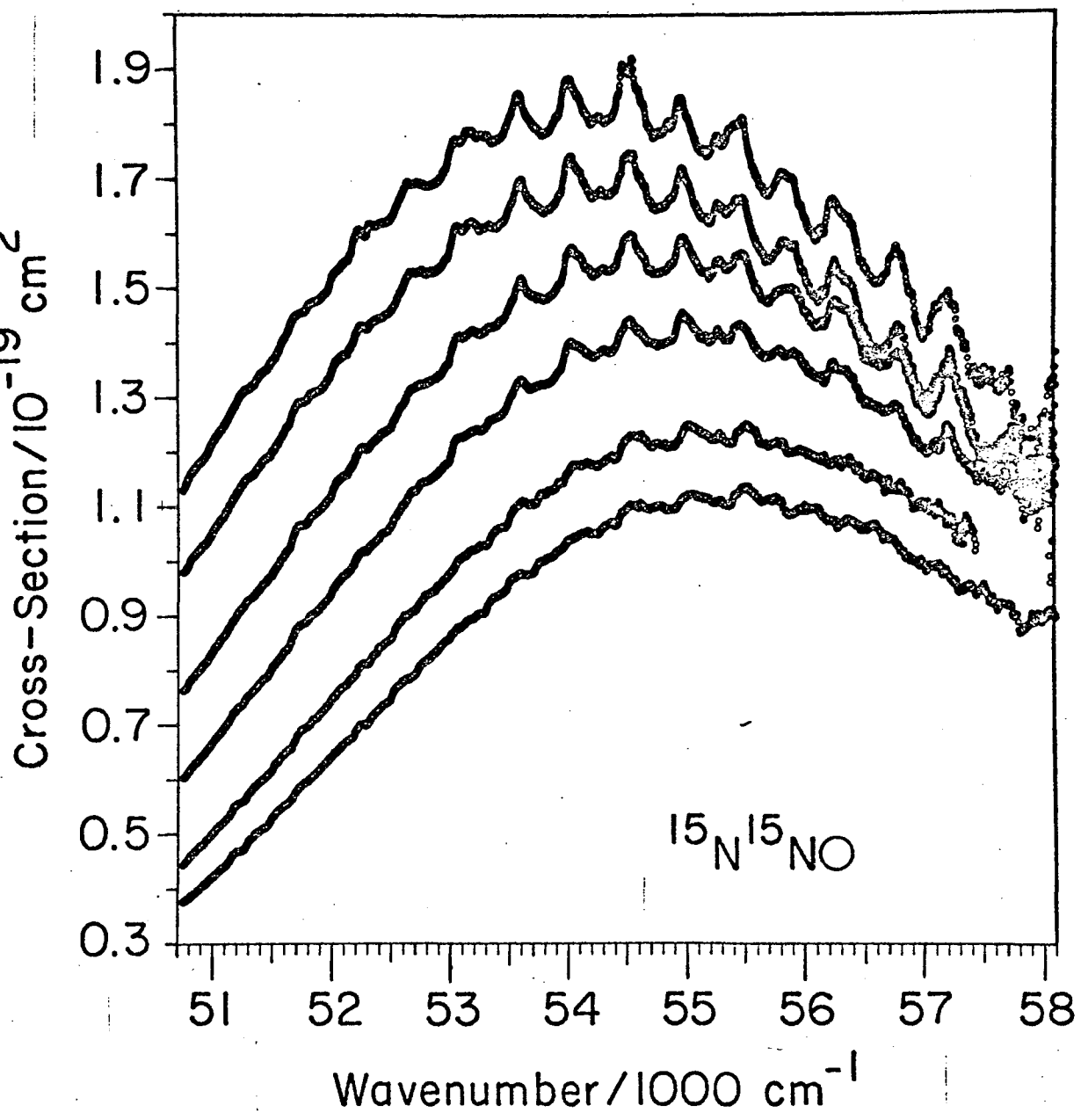
1.9
1.7
1.5
1.3
1.1
0.9
0.7
0.5
0.3
Cross-Section/10^{-19} cm^2
$^{15}N^{15}NO$
51
52
53
54
55
56
57
58
Wavenumber/1000 cm^{-1}

(6)

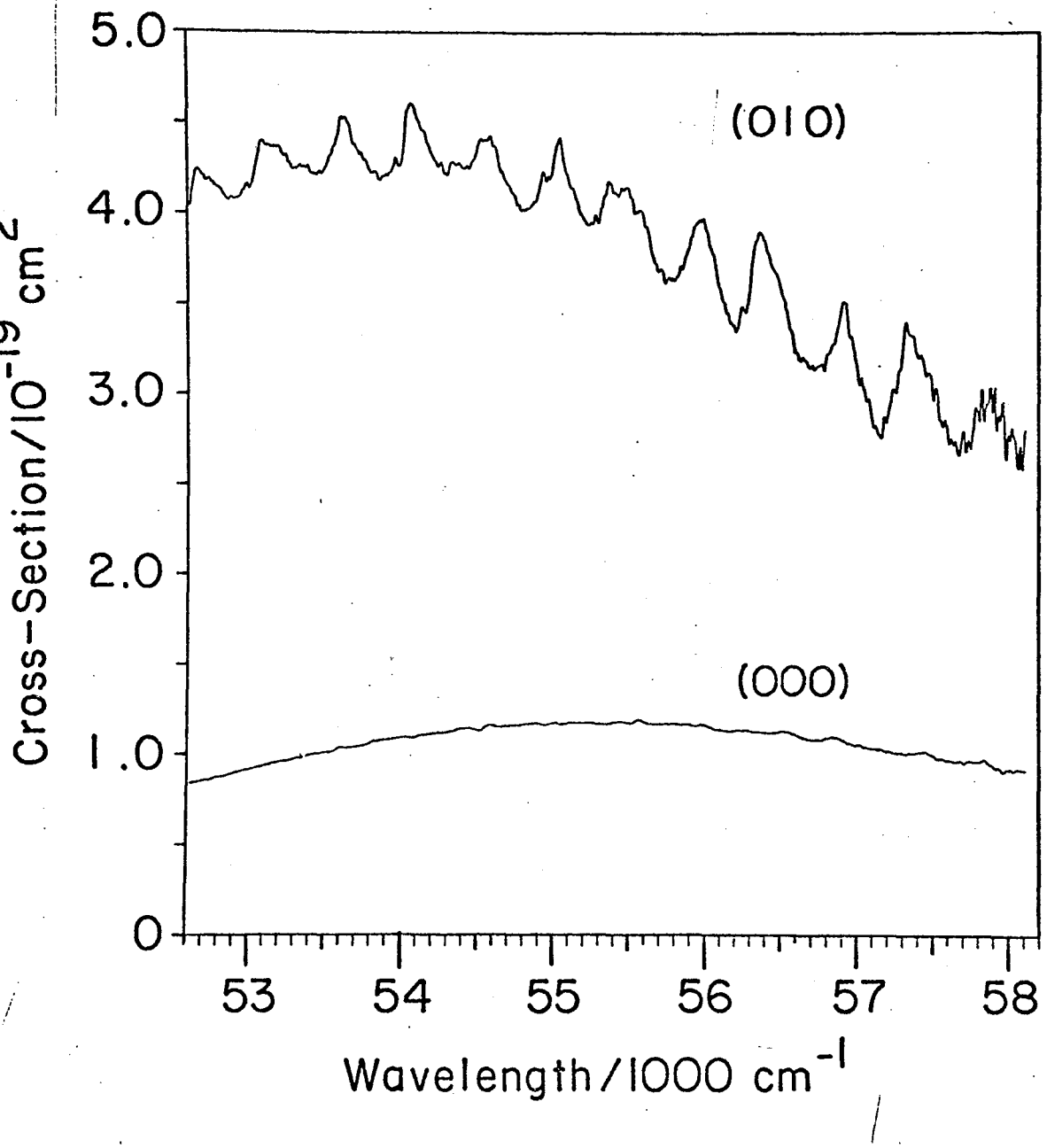
5.0
4.0
3.0
2.0
1.0
0
(010)
(000)
Cross-Section/10^{-19} cm^2
53
54
55
56
57
58
Wavelength/1000 cm^{-1}

(7)

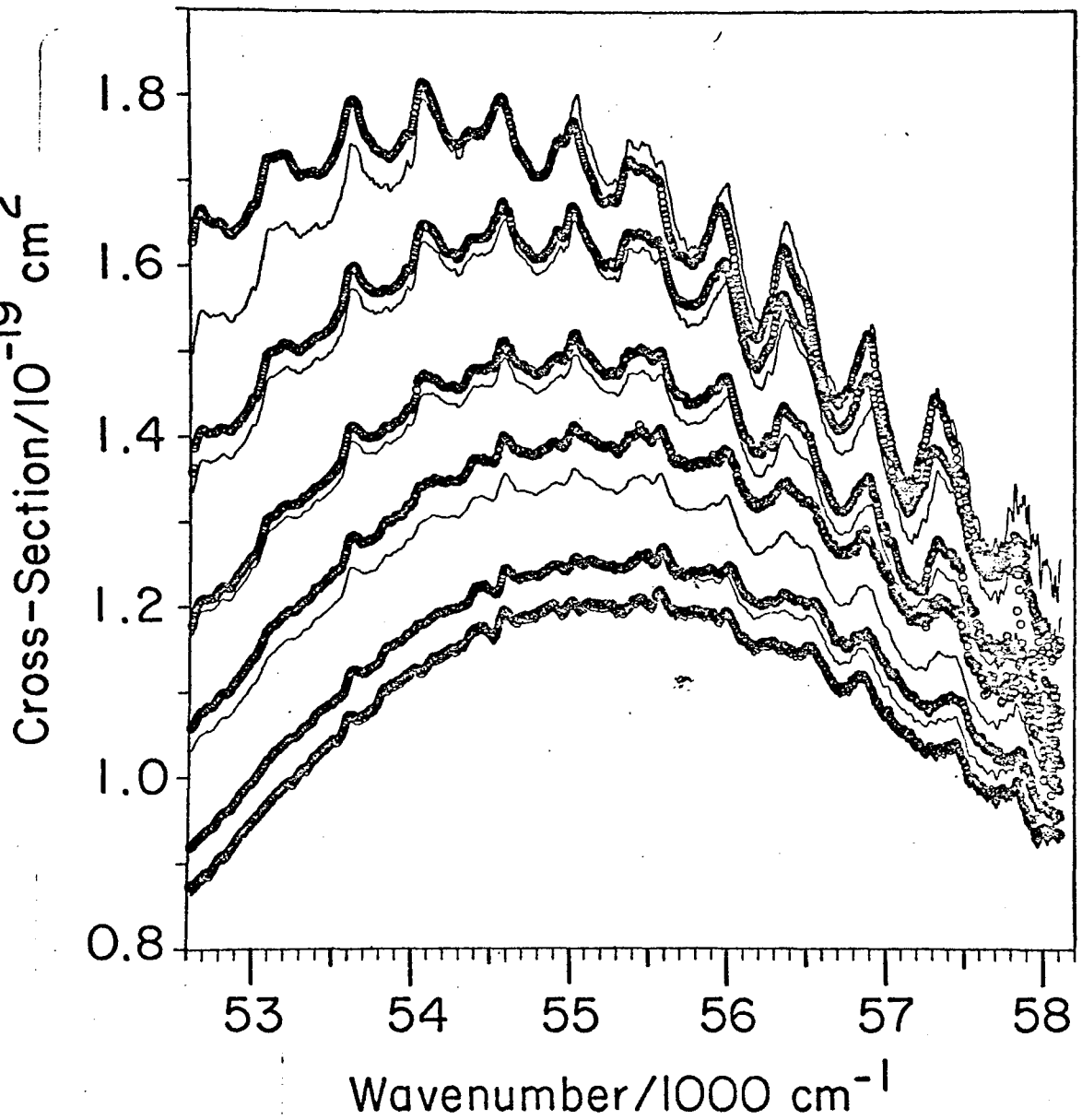
Cross-Section/10^{-19} cm^2
1.8
1.6
1.4
1.2
1.0
0.8
53
54
55
56
57
58
Wavenumber/1000 cm^{-1}

(8)

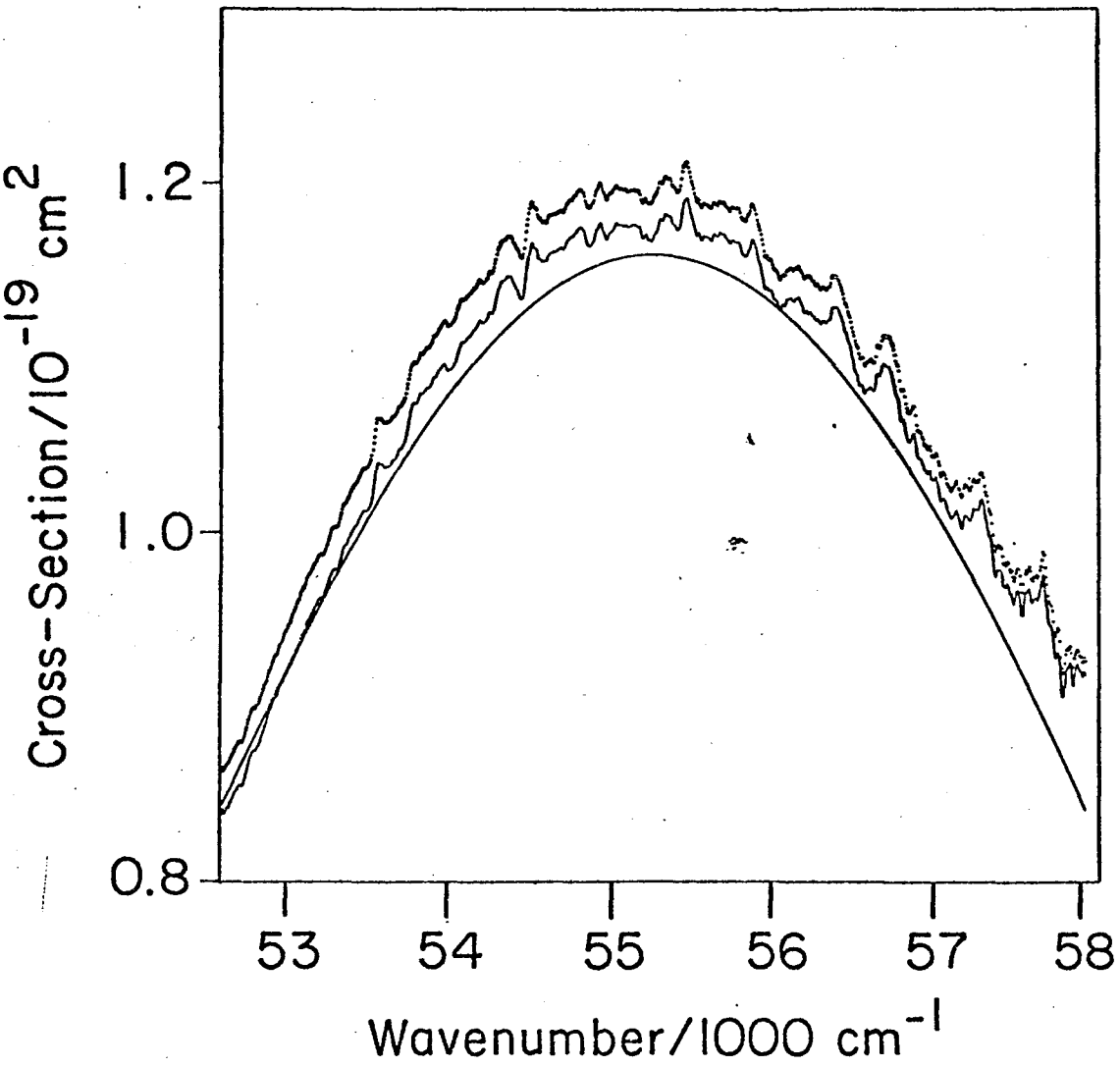
Cross-Section/10^{-19} cm^2
1.2
1.0
0.8
53
54
55
56
57
58
Wavenumber/1000 cm^{-1}

9

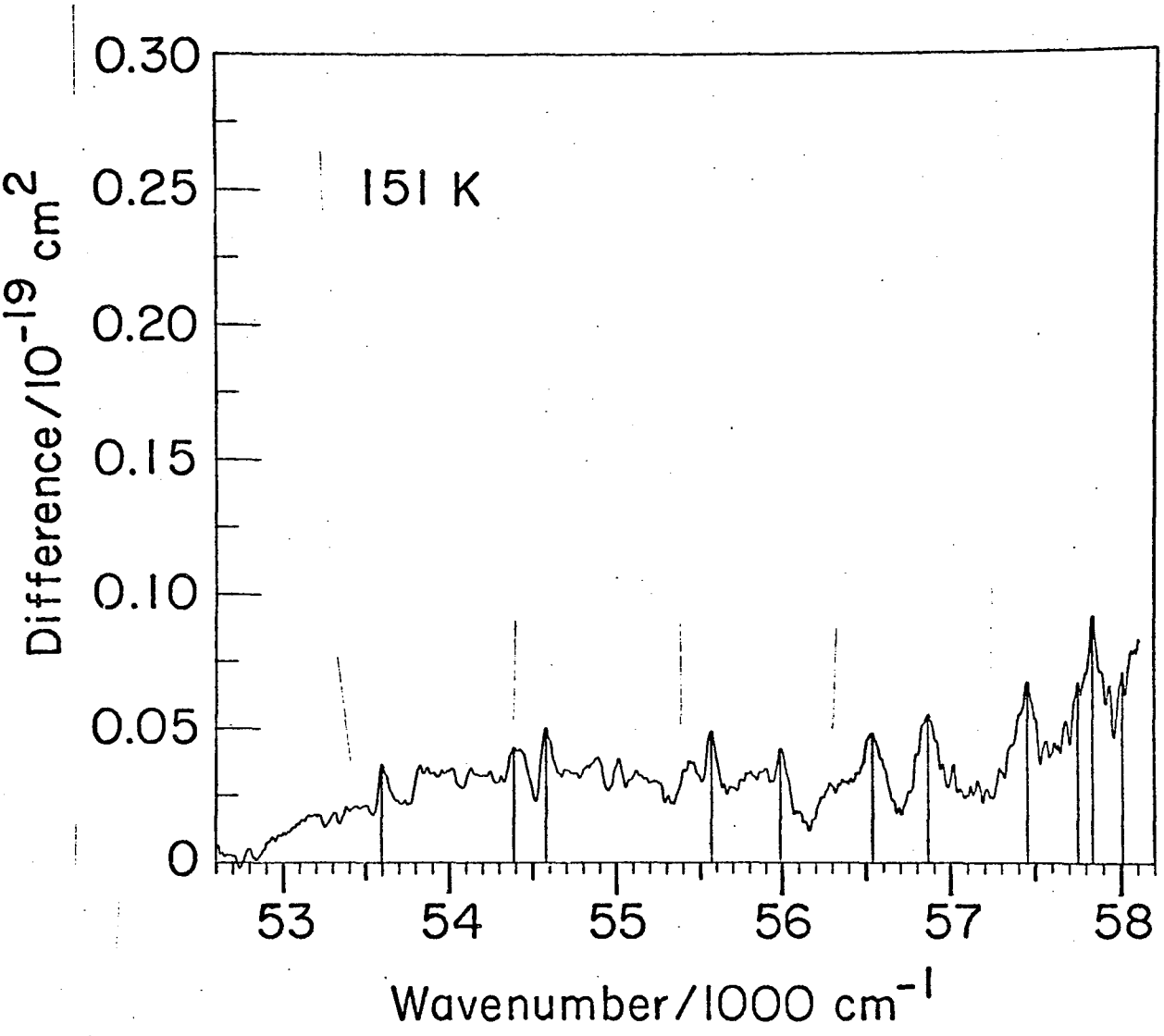
0.30
0.25
0.20
0.15
0.10
0.05
0
151 K
Difference/10^{-19} cm^2
53
54
55
56
57
58
Wavenumber/1000 cm^{-1}

(10)

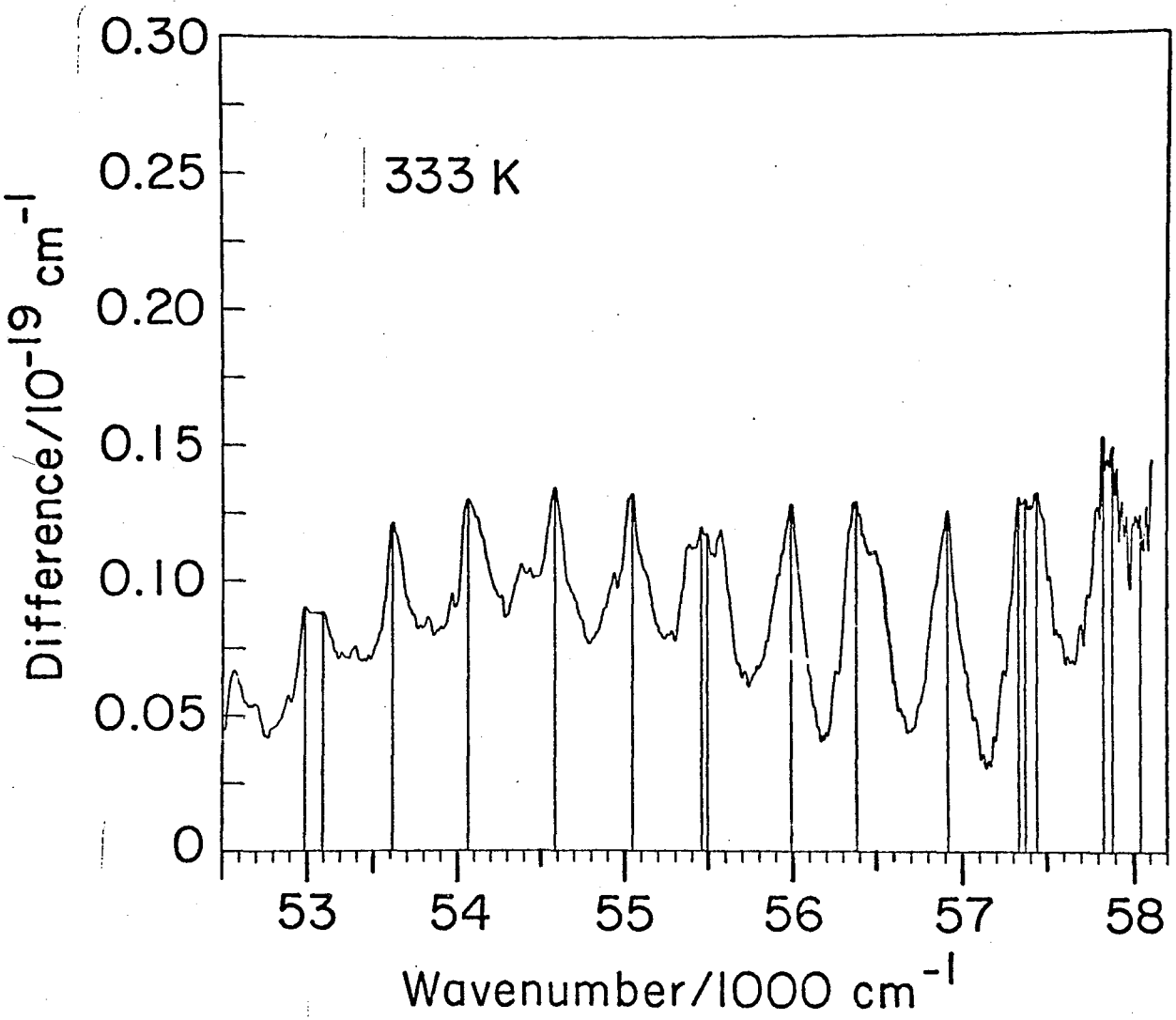
0.30
0.25
0.20
0.15
0.10
0.05
0
333 K
Difference/10^{-19} cm^{-1}
53
54
55
56
57
58
Wavenumber/1000 cm^{-1}

(11)

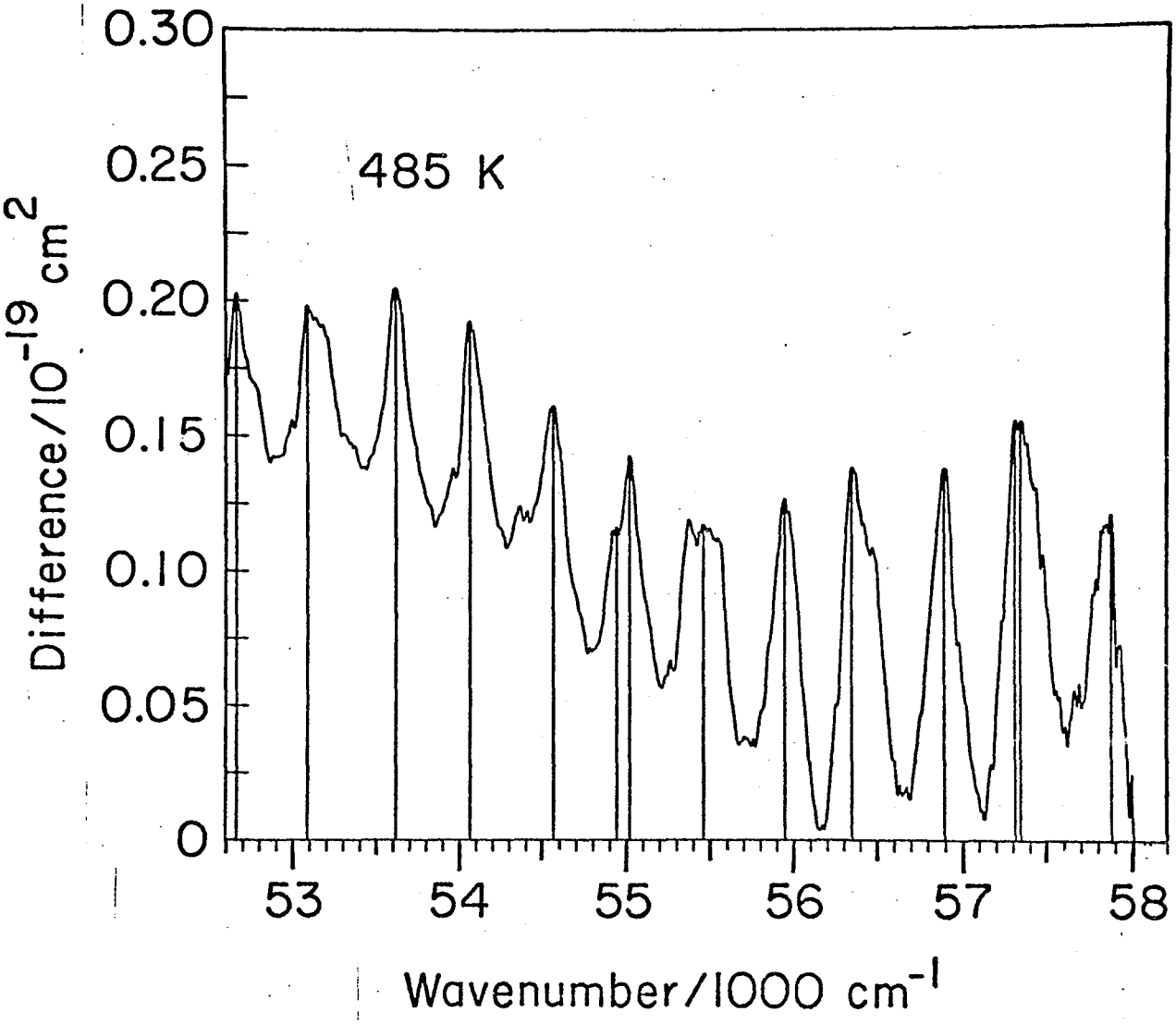
0.30
0.25
0.20
0.15
0.10
0.05
0
485 K
Difference/10^-19 cm^2
53
54
55
56
57
58
Wavenumber/1000 cm^-1

12

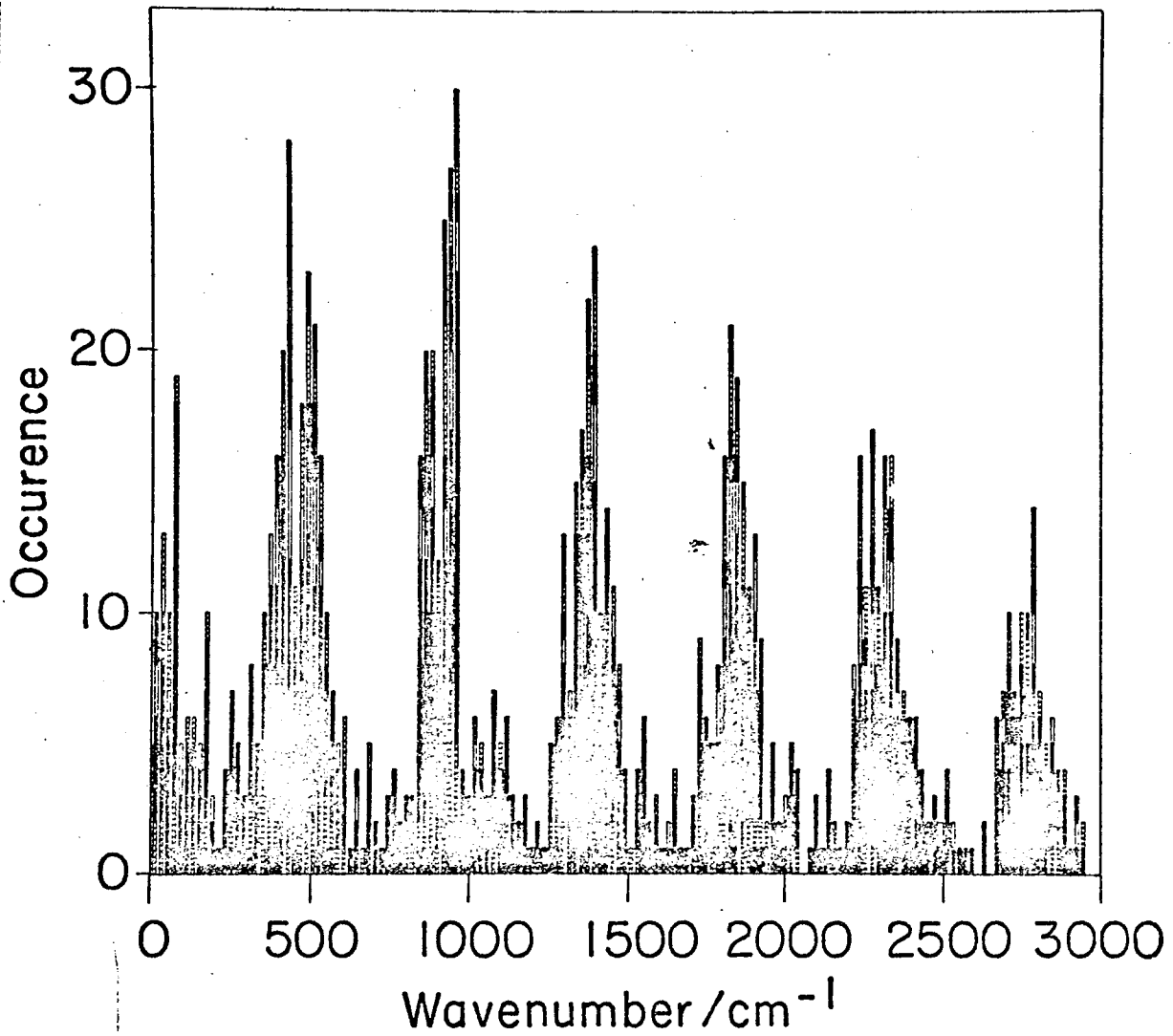
30
20
10
0
Occurence
0
500
1000
1500
2000
2500
3000
Wavenumber/cm⁻¹

(13)

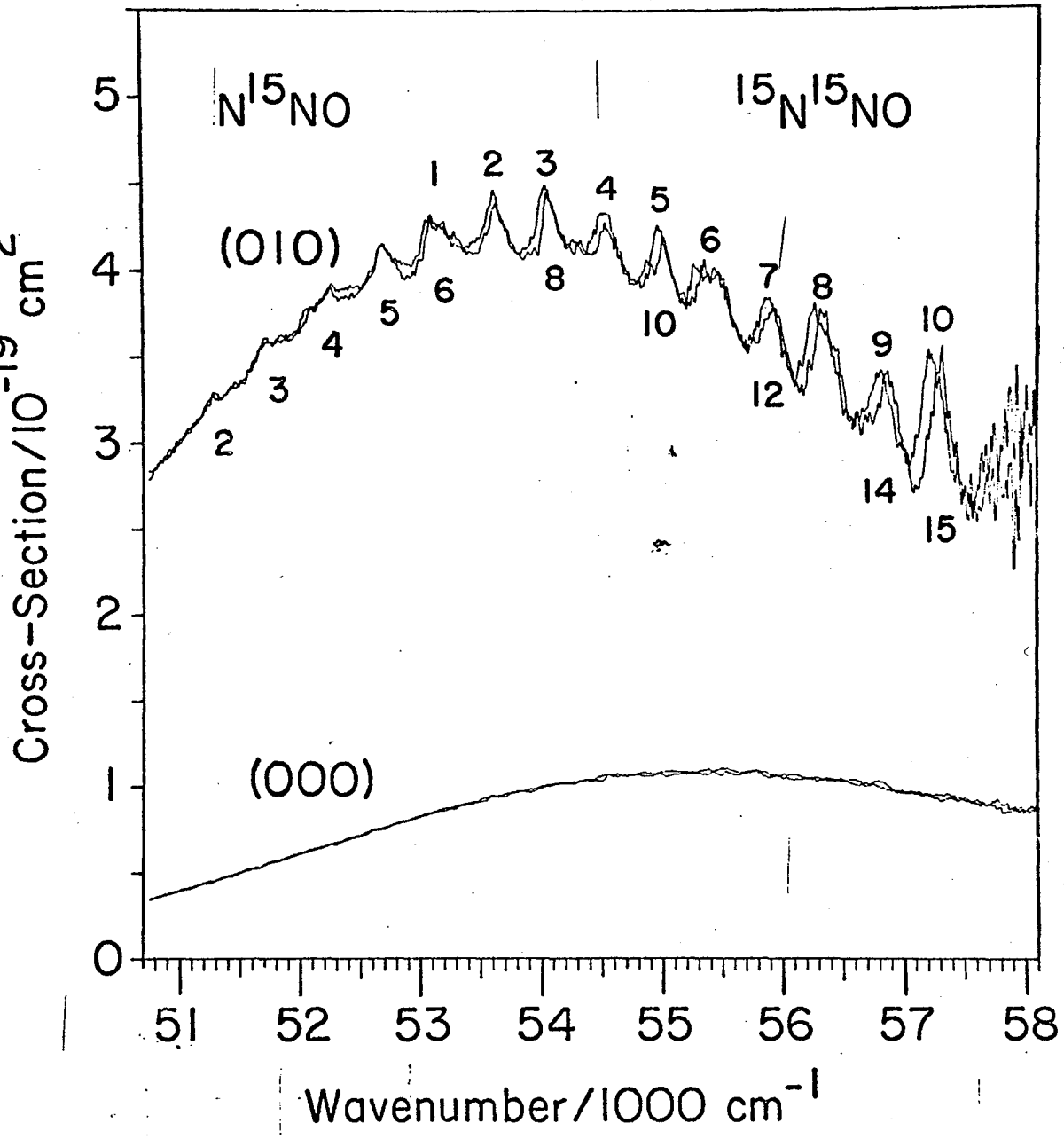
N15NO
15N15NO
(010)
(000)
1
2
3
4
5
6
7
8
9
10
12
14
15
Cross-Section/10-19 cm2
Wavenumber/1000 cm-1
0
1
2
3
4
5
51
52
53
54
55
56
57
58

14

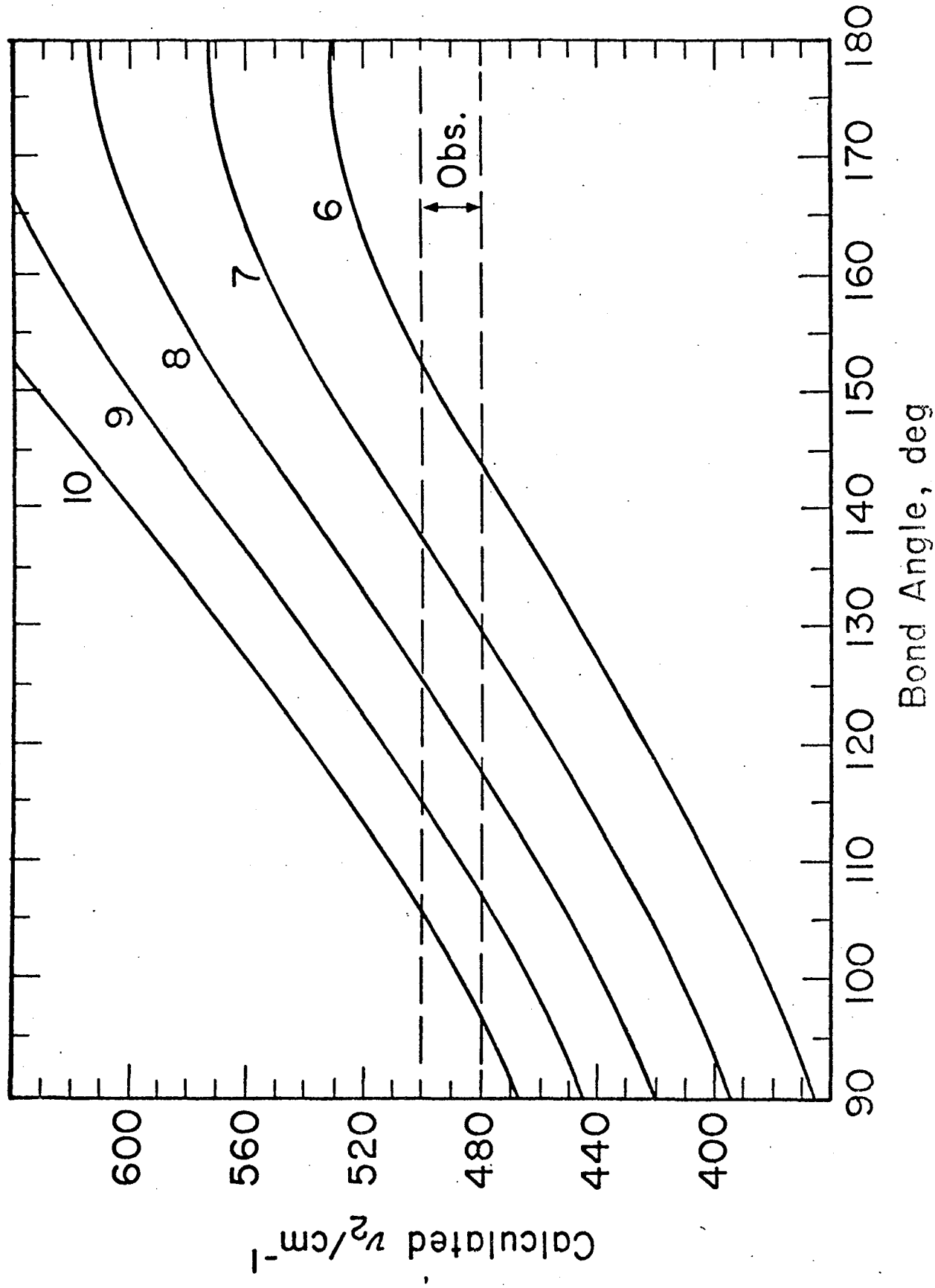
Calculated ν_2/cm^{-1}
600
560
520
480
440
400
90
100
110
120
130
140
150
160
170
180
Bond Angle, deg
Obs.
10
9
8
7
6

15

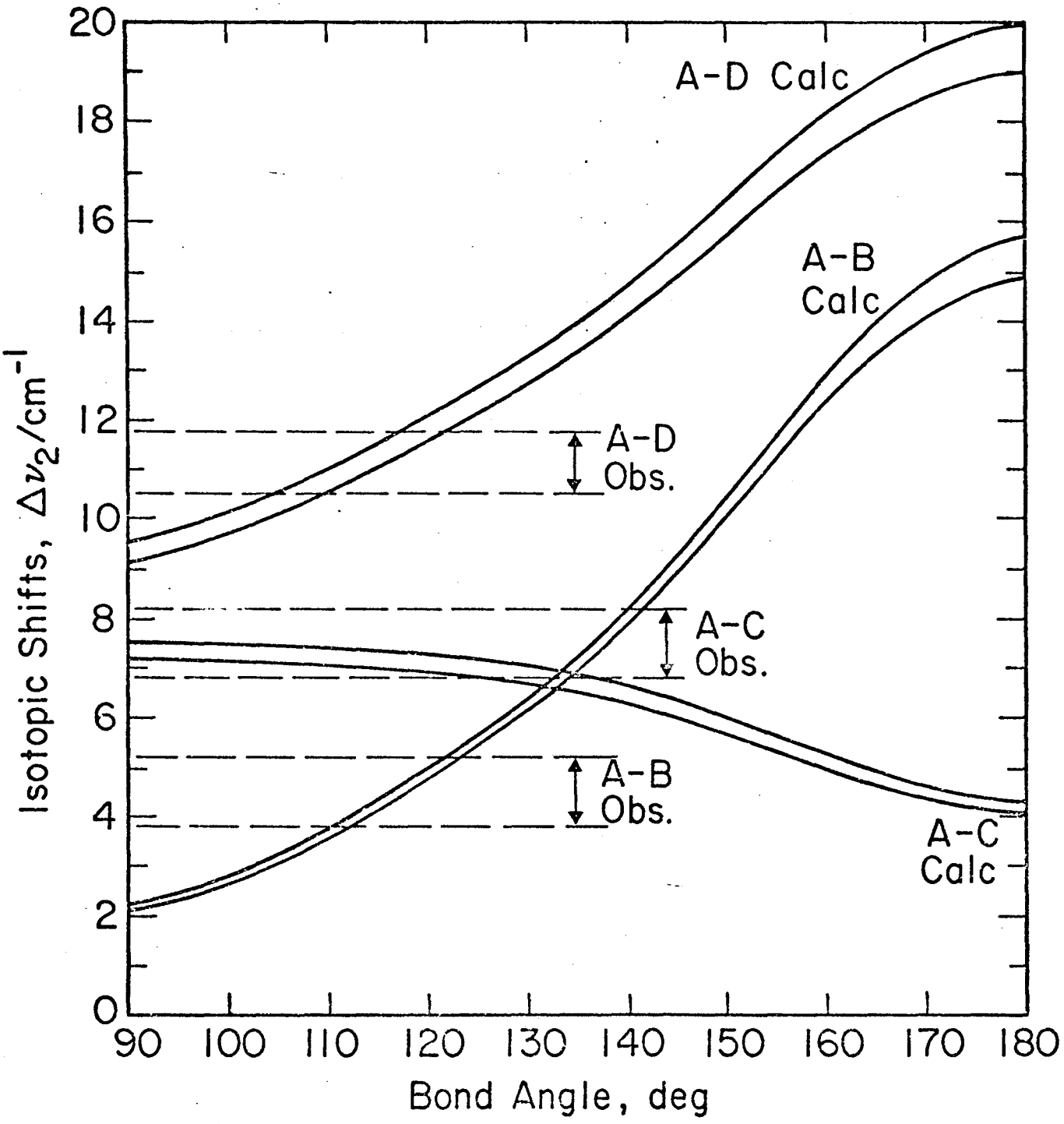
A-D Calc
A-B Calc
A-C Calc
A-D Obs.
A-C Obs.
A-B Obs.
Isotopic Shifts, $\Delta\nu_2/cm^{-1}$
Bond Angle, deg
0
2
4
6
8
10
12
14
16
18
20
90
100
110
120
130
140
150
160
170
180

16

This report was done with support from the United States Energy Research and Development Administration. Any conclusions or opinions expressed in this report represent solely those of the author(s) and not necessarily those of The Regents of the University of California, the Lawrence Berkeley Laboratory or the United States Energy Research and Development Administration.